

# Comparative morphology and postnatal ontogeny of the bony labyrinth in Pantherinae (Felidae, Carnivora) with special emphasis on the lion

**Festschrift in Honour of Professor Dr. Wolfgang Maier**

Edited by Ingmar Werneburg & Irina Ruf

Mathias Wirkner<sup>1,2</sup>, Katharina Heyder<sup>3</sup>, Irina Ruf<sup>1,2</sup>

1 *Abteilung Messelforschung und Mammalogie, Senckenberg Forschungsinstitut und Naturmuseum Frankfurt, Senckenberganlage 25, 60325 Frankfurt am Main, Germany*

2 *Institut für Geowissenschaften, Goethe-Universität Frankfurt am Main, Altenhöferallee 1, 60438 Frankfurt am Main, Germany*

3 *Technische Universität Dresden, Internationales Hochschulinstitut Zittau, Markt 23, 02763 Zittau, Germany*

<http://zoobank.org/References/CD8A71F5-9DDA-41FC-AA65-CDE6157A9580>

Corresponding author: Mathias Wirkner ([mathias.wirkner@senckenberg.de](mailto:mathias.wirkner@senckenberg.de))

**Academic editor** Ingmar Werneburg | **Received** 28 February 2022 | **Accepted** 29 June 2022 | **Published** 30 September 2022

**Citation:** Wirkner M, Heyder K, Ruf I (2022) Comparative morphology and postnatal ontogeny of the bony labyrinth in Pantherinae (Felidae, Carnivora) with special emphasis on the lion. *Vertebrate Zoology* 72 883–905. <https://doi.org/10.3897/vz.72.e82874>

## Abstract

The bony labyrinth (inner ear) of mammals reveals systematic as well as morphofunctional information. However, detailed knowledge of bony labyrinth morphology and ontogeny in Pantherinae, that comprise some of the most iconic mammals, is still pending. Hence, we present the first comparative description of the bony labyrinth in all extant species of *Panthera* and *Neofelis* some of which are represented by several postnatal stages; particular focus is set on *Panthera leo*. Our study is based on  $\mu$ CT scans and virtual 3D reconstructions and accompanied by selected morphometric measurements. Even though quite similar in morphology, both genera as well as their species can be distinguished by several features, e.g., shape and relative size of the semicircular canals and presence or absence of an osseous secondary crus commune. In case of the latter, *P. pardus* shows some intraspecific variation. We also traced the reduction of the fossa subarcuata during ontogeny in *P. leo* which conforms with previous studies. Negative allometry of the bony labyrinth in relation to skull basal length can be observed during ontogeny as demonstrated by *P. leo* as well as between different sized species. Although not correlated with the length of the cochlear canal, the number of cochlear turns is higher in captive non-adult *P. leo* and *P. tigris*, but lower in adult captive *P. pardus*. If these intraspecific differences are related to captivity or represent an ontogenetic pattern, needs to be evaluated in future studies based on larger samples.

## Keywords

fossa subarcuata, inner ear,  $\mu$ CT, *Neofelis*, *Panthera*, petrosal bone

## Introduction

The felid subfamily Pantherinae comprises the genera *Panthera* and *Neofelis*, which are found in a variety of habitats and characterized by different kinds of ecology, e.g., hunting and locomotion style as well as habitat (Nowak 1991; Sunquist and Sunquist 2002; Wilson and Mittermeier 2009; Davis et al. 2010; Billet et al. 2012, 2013; Pfaff et al. 2015, 2017; Schwab et al. 2019). Extant *Panthera* species comprise the lion (*P. leo*, Africa and Asia), the snow leopard (*P. uncia*, Asia), the leopard (*P. pardus*, Africa and Asia), the jaguar (*P. onca*, Central and South America), and the tiger (*P. tigris*, Asia) (Davis et al. 2010; Kitchener et al. 2017). These species can be sorted in two clades: the lion-leopard-jaguar clade (pantherine cats of African origin) and the tiger-snow leopard clade (pantherine cats of Asian origin) (Davis et al. 2010; Jiangzuo and Liu 2020). The clouded leopard (*Neofelis*) that is represented by two species in Asia (*N. nebulosa* and *N. diardi*) forms the sister-group of the *Panthera* species (Davis et al. 2010; Kitchener et al. 2017).

Though Pantherinae are omnipresent iconic animals in our culture, history and everyday life, significant gaps of knowledge concerning their intracranial structures still exist. This also holds true for the inner ear, which comprises the auditory sensory organ and the vestibular system. The membranous inner ear is housed in the bony labyrinth of the petrosal bone, that reflects size and shape of the soft tissue and therefore can be used for investigation of macerated skulls and fossil specimens (Johnsson and Hawkins 1967; Ekdale 2016). Several authors associate the shape of the bony labyrinth with ecological and phylogenetic information of extant species. Hence, bony labyrinth morphology and morphometry can serve as a functional and ecological proxy but also provides characters for phylogenetic analyses in extant and extinct mammals (e.g., Spoor et al. 2007; Billet et al. 2012, 2013; Pfaff et al. 2015, 2017; Mennecart et al. 2016; Schwab et al. 2019).

Previous studies on the inner ear and/or bony labyrinth that also include members of Pantherinae are restricted to selected species that are mostly used for comparison as part of a larger sample. *Panthera leo* (Spoor et al. 2007; Pfaff et al. 2017; Schwab et al. 2019) and *Panthera tigris* (Burda et al. 1984; Úlehlová et al. 1984; Spoor et al. 2007; Grohé et al. 2018; Schwab et al. 2019) are the most prominent species, followed by *Panthera pardus* (Pfaff et al. 2017; Grohé et al. 2018), *Panthera onca* (Burda et al. 1984; Úlehlová et al. 1984) and *Neofelis nebulosa* (Grohé et al. 2018). To our knowledge, there is no published data of the bony labyrinth of *Panthera uncia* and *Neofelis diardi*. Furthermore, these studies focus on morphological details of the membranous inner ear (organ of Corti) and the morphometry of the vestibular system. Even though there are some morphological descriptions of the bony labyrinth of the domestic cat (*Felis catus*) (Ekdale 2013; Schellhorn 2018), and other Felinae (Etmayr 2014), detailed descriptions of the inner ear morphology of Pantherinae species are still pending.

However, for the deeper understanding of the morphology and morphofunction of intracranial structures associated with sensory organs, it is important to investigate their ontogeny (Maier and Ruf 2014). Early ontogenetic stages may reveal insights into selective pressure that leads to functional adaptations of the respective organ (Perier et al. 2016). To date only few studies on the ontogeny of the bony labyrinth exist, most of which are restricted to selected non-pantherine species (e.g., Morsli et al. 1998; Jeffery and Spoor 2004; Sánchez-Villagra and Schmelzle 2007; Ekdale 2010; Costeur et al. 2017; Berlioz et al. 2021); comparative ontogenetic studies on pantherine skulls are limited to external structures (Segura et al. 2017).

Hence, we present the first detailed morphological description of the bony labyrinth of all extant Pantherinae species. In addition, for the first time, the postnatal ontogeny of the bony labyrinth of *P. leo* and to some extent of *P. tigris* and *P. pardus* is described. Selected morphometric data are used for interspecific comparison and evaluation of ontogenetic transformations.

## Methods

### Material

Based on  $\mu$ CT scans of macerated skulls, the bony labyrinth of seven lions (*Panthera leo*), three tigers (*P. tigris*), three leopards (*P. pardus*), one jaguar (*P. onca*), one snow leopard (*P. uncia*), one Sunda clouded leopard (*Neofelis diardi*) and one mainland clouded leopard (*N. nebulosa*) were studied. All species are represented by adult stages; the studied *P. leo*, *P. tigris* and *P. pardus* sample comprises also younger ontogenetic stages (Table 1). All specimens are housed in the mammal collection of the Senckenberg Forschungsinstitut und Naturmuseum Frankfurt, Germany. Our sample comprises wild as well as captive specimens. Early ontogenetic stages of wild specimens are rare in scientific collections and we could only include captive individuals, although the older ontogenetic stage sample comprises both origins. Thus, we could separate intra- and/or interspecific differences from ontogenetic differences and/or captivity effects. Specimens were chosen for overall condition (i.e., completeness of internal structures, quality of preparation) and available data on origin (wild versus captive) were considered if available. The studied specimen of *Neofelis diardi* (SMF15470) is a special case. It was caught presumably as an adult on Sumatra and brought to Zoo Frankfurt in 1955, where it died a few months later. Hence we considered its origin as wild.

Former studies showed, that due to functional constraints no significant intraspecific and intraindividual variation of the bony labyrinth should be present in fast-moving species, as which we categorize Pantherinae (i.e., Spoor et al. 2007), and thus even a single specimen allows for evaluation (e.g., Billet et al. 2012; Perier et al.

**Table 1.** Pantherinae specimens considered in the present study. Subspecies are assigned according to recent taxonomy (Kitchener et al. 2017). “?” illustrates unknown or, following an subspecies name or origin, uncertainty (assumption based on available metadata). “—” means non-existent.

Genus	Species	Subspecies	Specimen	Source	Origin	Age	IDAS (modified)
<i>Panthera</i>	<i>leo</i>	?	SMF 95010	Zoo Frankfurt	captive	neonate	1.1
<i>Panthera</i>	<i>leo</i>	?	SMF 15765	Zoo Frankfurt	captive	juvenile	1.2
<i>Panthera</i>	<i>leo</i>	?	SMF 38325	?	?	juvenile	1.3
<i>Panthera</i>	<i>leo</i>	<i>melanochaita</i>	SMF 4643	Faradje, Democratic Republic Congo, Africa	wild	adult	3
<i>Panthera</i>	<i>leo</i>	?	SMF 22101	Northeast Africa	wild	adult	3
<i>Panthera</i>	<i>leo</i>	?	SMF 22104	Northeast Africa	wild	adult	3
<i>Panthera</i>	<i>leo</i>	<i>leo?</i>	SMF 1366	Batavia (today Jakarta, Indonesia)	wild?	adult	3
<i>Panthera</i>	<i>pardus</i>	<i>pardus</i>	SMF 15745	Daroli, Arsi Province, Ethiopia, Africa	wild	juvenile	1.2
<i>Panthera</i>	<i>pardus</i>	<i>pardus</i>	SMF 16259	Africa	wild	adult	3
<i>Panthera</i>	<i>pardus</i>	?	SMF 94342	Zoo Frankfurt	captive	adult	3
<i>Panthera</i>	<i>pardus</i>	<i>orientalis?</i>	SMF 95992	Zoo Frankfurt	captive	adult	3
<i>Panthera</i>	<i>onca</i>	?	SMF 3067	Paramaribo, Republic of Suriname, South America	wild	adult	3
<i>Panthera</i>	<i>tigris</i>	<i>tigris</i>	SMF 15722	Zoo Frankfurt	captive	neonate	1.1
<i>Panthera</i>	<i>tigris</i>	<i>sondaica</i>	SMF 15737	Java, Indonesia	wild?	adult	3
<i>Panthera</i>	<i>tigris</i>	<i>sondaica</i>	SMF 7020	Bunga-Bonda, Sumatra, Indonesia	wild	adult	3
<i>Panthera</i>	<i>tigris</i>	<i>sondaica</i>	SMF 92259	Zoo Frankfurt	captive	adult	3
<i>Panthera</i>	<i>uncia</i>	?	SMF 5419	Ferghana / Farg'ona, Farghona Wiloyati, Uzbekistan	wild	adult	3
<i>Neofelis</i>	<i>diardi</i>	<i>diardi?</i>	SMF 15470	Zoo Frankfurt, from Sumatra, Indonesia	wild (captive)	adult	3
<i>Neofelis</i>	<i>nebulosa</i>	—	SMF 40850	Zoo Frankfurt	captive	adult	3

2016; Cerio and Witmer 2019; Gonzales et al. 2019). However, in some species a certain level of plasticity of the bony labyrinth has been observed (Ekdale 2010, 2016). When possible we also investigated both bony labyrinths of a specimen. For better comparison, we mirrored the left bony labyrinths.

We used the individual dental age stages (IDAS) of Anders et al. (2011) for assigning the studied specimens to the age groups infant (IDAS 1) and adult (IDAS 3). According to Anders et al. (2011) all subadult *P. leo* specimens in our sample are categorized as infant although differing in size and age. In order to discriminate these specimens, we used the eruption sequence of the teeth according to Smuts et al. (1978) as well as the skull basal length of the skull and modified the IDAS system accordingly (Table 1). The three lion infants could be sorted from youngest (neonate) to oldest as follows: SMF 95010 has no erupted teeth at all and the smallest skull (IDAS 1.1), SMF 15765 has premolars but no lower M1 and a bigger skull (IDAS 1.2). SMF 38325 has a not fully erupted lower M1 and the biggest skull of these three specimens (IDAS 1.3).

The skull of the neonate *P. tigris* (SMF 15722) is most similar in size, cranial development and tooth development to the neonate *P. leo* (SMF 95010) and therefore assigned to IDAS 1.1. The infant *P. pardus* (SMF 15745) is in a similar tooth eruption sequence stage as SMF 15765 and therefore assigned to IDAS 1.2.

Body mass is taken from literature (Wilson and Mittermeier 2009); due to missing data on sex in many specimens we used the mean body mass value for the respective

species. *P. leo* = 127.25 kg, *P. pardus* = 55 kg, *P. onca* = 72.25 kg, *P. tigris sondaica* = 106.25 kg, *P. uncia* = 37 kg, *Neofelis diardi* = 17.5 kg, *N. nebulosa* = 17 kg. Carnivora taxonomy is based on Wilson and Mittermeier (2009) and the phylogeny of Pantherinae on Davis et al. (2010).

For outgroup comparison, bony labyrinths of further Carnivora from literature (i.e., *Acinonyx jubatus*, *Canis lupus familiaris*, *Caracal caracal*, *Eumetopias jubatus*, *Felis catus*, *Felis chaus*, *Priolainurus viverrinus*, *Puma concolor*) were taken into account (Ekdale 2013; Etmayr 2014; Grohé et al. 2018; Schellhorn 2018).

## μCT scans and virtual 3D reconstructions

Tomographic data were obtained with the μCT scanner GE phoenix x|ray v|tome|x s that is housed at the Institut für Geowissenschaften und Meteorologie, Rheinische Friedrich-Wilhelms-Universität Bonn, Germany. The *P. tigris* SMF 15737 specimen was scanned with an Xylon FF 85 CT located at Xylon International GmbH, Hamburg, Germany. See Table S1 for details on scan parameters. In order to increase the resolution, the voxel size of some scans was virtually halved (voxel size res 2) during reconstruction of the raw data by applying the res2 tool of the software datos|x reconstruction (GE Sensing & Inspection Technologies GmbH) (Luo et al. 2012). Image stacks (.jpg or .tiff) of the μCT scans were created using VGStudio MAX® 2.2 (Volume Graphics GmbH, Heidelberg, Germany). Digital endocasts were created in Ami-

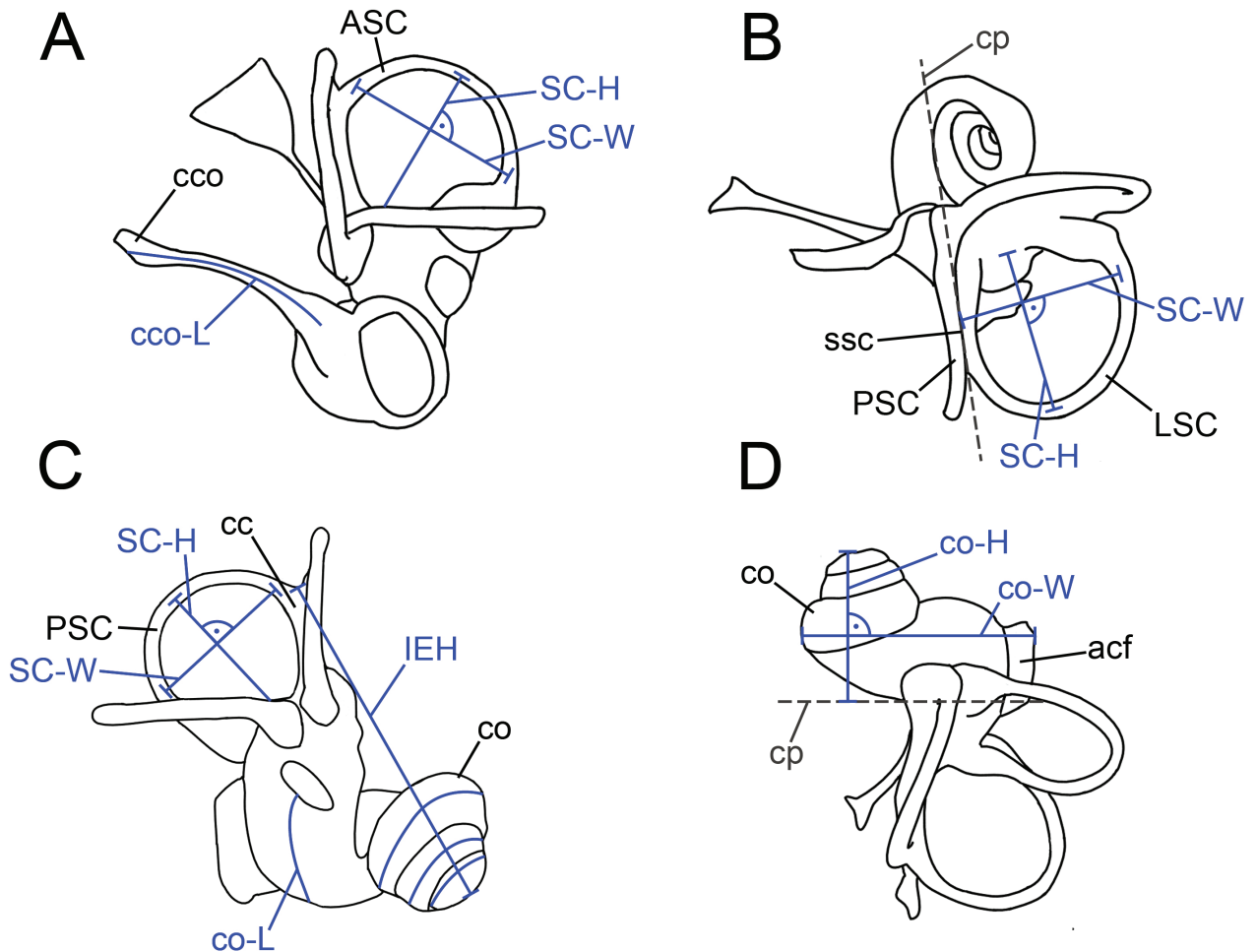


**Figure 1.** Linear measurements (blue) exemplified on the right bony labyrinth of an adult *Panthera leo* (SMF 4643) in posterolateral (A), dorsal (B), anterolateral (C) and dorsolateral (D) view. Abbreviations: acf, aperture of the cochlear fossula; ASC, anterior semicircular canal; cco, canaliculus cochleae; cco-L, canaliculus cochleae length; co, cochlea; co-H, cochlear height; co-L, cochlear length; co-W, cochlear width; cp, clipping plane; fv, fenestra vestibuli; IEH, inner ear height; LSC, lateral semicircular canal; PSC, posterior semicircular canal; ssc, secondary crus commune; SC-H, semicircular canal height; SC-W, semicircular canal width.

ra<sup>®</sup> 5.4.0 and Avizo<sup>®</sup> 9.0.1 (Thermo Fisher Scientific FEI, Waltham, MA USA). Segmentation of the relevant bone cavities (virtual endocasts) was done with various tools (i.e., brush and magic wand) resulting in unsmoothed 3D digital endocasts.

## Morphometric measurements

Morphological observations are supported by selected morphometric measurements on the bony labyrinth. Each measurement was conducted three times and a mean value was calculated (Table 2, for raw measurements see Table S2). In order to delete the effect of body size, especially when comparing different ontogenetic stages, variables were divided by the skull basal length. Skull basal length was measured, using a calliper, from the most anterior point of the premaxillary bone (prosthion) to the most anterior point of the anterior rim of the foramen magnum (basion) (Crégut-Bonnoure et al. 2018). Because of the condition of the skull of *P. pardus* SMF 15745, it was not possible to measure its skull basal length. We estimated

the skull basal length to be approximately 110 mm, but we chose to exclude it from the analysis, when skull basal length was considered (Table 2).

Unless otherwise stated, the following measurements were conducted digitally in Avizo<sup>®</sup> 9.0.1/Avizo<sup>®</sup> 9.0.1 Lite. For calculating the radius of curvature of each semicircular canal, measurements are taken based on the protocol by Schmelzle et al. (2007) using height (H), width (W) and the formula  $r = 0.5(H+W)/2$ . Maximum height was defined as the longest distance within the plane of the respective semicircular canal between its inner curvature and the vestibule. Maximum width was determined as the maximum length perpendicular to the maximum height (Fig. 1A, B, C). Modification of the protocol according to Ruf et al. (2016) allows comparison with data in Spoor et al. (2007): In order to measure the maximum distance from the vestibule to the center of the canal, the mean of measurements for inner and outer curvature was calculated. The same adjustments are done for the maximum perpendicular width. In cases where the posterior semicircular canal was fused to the lateral canal in the area of measurement, a clipping plane was used to cut off the posterior

**Table 2.** Measurements and indices of the bony labyrinth in the studied Pantherinae sample. Asterisk (\*) indicates that the ASC-R of *Neofelis nebulosa* could not be measured exactly due to partial exposure of the canal (see description). Abbreviations: ASC, anterior semicircular canal; BL, skull basal length; cco, canaliculus cochleae; co, cochlea; IEH, inner ear height; L, length; l, left; LSC, lateral semicircular canal; PSC, posterior semicircular canal; R, radius of curvature; r, right; sbl, secondary bony lamina; SC, semicircular canals (mean); A, approximation, because the foramen magnum was damaged in this specimen.

Genus	Species	Specimen	IDAS (modified)	BL (mm)	IEH (mm)	IEH/BL	ASC-R (mm)	LSC-R (mm)	PSC-R (mm)	SC-R (mm)	co-L (mm)	cco-L (mm)	co aspect ratio	co turns	Length of sbl regarding first co turn
<i>Panthera</i>	<i>leo</i>	SMF 95010	1.1	64.87	13.937	0.215	3.133	2.786	2.790	2.903	48.565	2.875	0.668	3.25	<1/2
<i>Panthera</i>	<i>leo</i>	SMF 15765	1.2	138.57	13.677	0.099	2.997	2.635	2.968	2.867	50.735	6.740	0.608	3.25	~1/2
<i>Panthera</i>	<i>leo</i>	SMF 38325	1.3	251.72	13.691	0.054	3.249	2.739	2.877	2.955	49.687	8.828	0.647	3.25	~1/3
<i>Panthera</i>	<i>leo</i>	SMF 4643	3	264.63	13.545	0.051	3.285	3.000	3.163	3.149	47.843	8.590	0.621	3.25	<1/2
<i>Panthera</i>	<i>leo</i>	SMF 22101	3	233.45	12.303	0.053	3.017	2.898	3.009	2.974	46.596	7.393	0.525	3	<1/2
<i>Panthera</i>	<i>leo</i>	SMF 22104	3	240.68	13.286	0.055	3.227	3.090	2.977	3.098	46.563	8.000	0.579	2.75	~1/3
<i>Panthera</i>	<i>leo</i>	SMF 1366	3	280.77	14.113	0.050	3.387	2.935	3.281	3.201	51.733	7.330	0.574	3	—
<i>Panthera</i>	<i>pardus</i>	SMF 15745	1.2	110 <sup>A</sup>	10.814	—	2.807	2.615	2.797	2.740	42.430	—	—	3.5	~1/2
<i>Panthera</i>	<i>pardus</i>	SMF 16259 r	3	181.52	12.465	0.069	3.015	2.558	2.740	2.771	47.076	—	—	3.25	<1/2
<i>Panthera</i>	<i>pardus</i>	SMF 16259 l	3	181.52	12.528	0.069	3.063	2.680	2.705	2.816	47.362	—	—	3.25	—
<i>Panthera</i>	<i>pardus</i>	SMF 94342	3	197.43	11.347	0.057	2.807	2.615	2.797	2.740	44.723	—	—	3	—
<i>Panthera</i>	<i>pardus</i>	SMF 95992	3	186.45	12.290	0.066	3.179	2.775	3.126	3.027	46.409	—	—	3	—
<i>Panthera</i>	<i>onca</i>	SMF 3067	3	194.42	13.856	0.071	3.197	2.742	2.785	2.908	50.523	—	—	3.5	<1/2
<i>Panthera</i>	<i>tigris</i>	SMF 15722	1.1	63.72	13.596	0.213	3.200	2.831	3.021	3.017	52.196	3.001	—	3.25	>1/2
<i>Panthera</i>	<i>tigris</i>	SMF 15737	3	235.18	13.128	0.056	3.039	2.815	2.731	2.862	50.940	7.900	—	3	<1/2
<i>Panthera</i>	<i>tigris</i>	SMF 7020	3	239.45	14.540	0.061	3.235	2.908	3.086	3.076	52.322	6.280	—	3	—
<i>Panthera</i>	<i>uncia</i>	SMF 5419	3	154.15	10.782	0.070	2.826	2.561	2.521	2.636	38.074	—	—	3	—
<i>Neofelis</i>	<i>diardi</i>	SMF 15470	3	116.93	10.570	0.090	2.675*	2.285	2.429	2.463	42.307	—	—	3	<1/2
<i>Neofelis</i>	<i>nebulosa</i>	SMF 40850	3	130.30	10.000	0.077	2.523	2.142	2.272	2.312	40.208	—	—	3.25	<3/4

semicircular canal in the area of the osseous secondary crus commune to measure the outer width of the lateral semicircular canal (Fig. 1B). Additionally, in some cases the outer curvature of the anterior and/or posterior semicircular canal was measured by passing through the crus commune.

The length of the canaliculus cochleae of *P. leo* was measured using the SplineProbe tool (Fig. 1A). The digital endocasts were rendered transparent and SplineProbe anchor points were placed in varying distances in the center of the canal from its base to its end.

In order to measure the width of the cochlea, the greatest distance from the vestibular/ventral edge of the aperture of the cochlear fossula to the radial wall of the opposite side of the basal cochlear turn parallel to the plane of the latter was measured (Ekdale 2010; Ekdale and Rowe 2011; Fig. 1D).

The height of the cochlea was measured perpendicular to the width of the cochlea as the greatest distance from the apex of the spiral to the plane at the level of the tympanal/dorsal edge of the aperture of the cochlear fossula. This plane was parallel to another plane which went through the basal turn of the cochlear canal (Ekdale 2010; Ekdale and Rowe 2011; Fig. 1D). Following this, a shape index of the cochlea, the aspect ratio, was calculated by dividing the height of the cochlea by the width of the cochlea. Previous studies considered an aspect ratio of above 0.55 as high or “sharp-pointed” while an aspect ratio of 0.55 and below is considered “flattened” (Ekdale 2013 and references therein).

The cochlea length was measured by using the surface pathway tool. It is measured along the outer curvature of the spiral, starting from the anterior border of the fenestra vestibuli up to the apex of the cochlea (Ruf et al. 2009, 2016; Schwarz 2012; Fig 1C). There are other methods using the spline probe tool starting at the beginning of the laminar gap up to the apex of the cochlea (Ekdale 2010; Ekdale and Rowe 2011). However, the secondary bony lamina was not visible in all studied specimens, therefore we favored the approach described above. In order to count the number

of cochlear turns the digital endocast was aligned in apex view. A line is drawn from the inflection point of the fenestra vestibuli to the apex of the cochlear canal (West 1985; Ruf et al. 2016). In the same way the length of the secondary bony lamina was measured.

For the inner ear height (IEH) the linear distance between the dorsal apex of the crus commune and the ventral apex of the cochlea was measured as described by Billet et al. (2013) (Fig. 1C).

## Regression analyses

For the regression analyses we only used adult specimens. In addition, we excluded the right bony labyrinth of SMF 16259, for using only one bony labyrinth from each specimen. Linear regressions were initially done in Microsoft excel® 2010 and PAST 4.03 (Hammer et al. 2001; Hammer 2020). The base figures from excel were then enhanced in Adobe Illustrator® CS5.

## Results

In the following, the bony labyrinth of *Panthera leo* is described in detail first. This description serves as a base for comparison with all other pantherine species.

### Morphological and morphometric description of *Panthera leo*

Overall, the individual bony labyrinths of the *Panthera leo* specimens across different ontogenetic stages are quite similar (Figs 2, S1). The main differences arise from the shape and proportional length of the canaliculus cochleae and aquaeductus vestibuli, as well as the number of cochlear turns. The mean inner ear height (IEH), that represents bony labyrinth size, of all *P. leo* specimens combined is 13.508 (+/-0.550) mm. Correcting the distinct IEH values for skull basal length a negative allometry from the infant to the adult specimens becomes apparent (Fig. 3A).

The curvature of the semicircular canals is round to oval with only slight undulation. The vestibular apparatus and cochlea are roughly evenly proportioned.

The anterior semicircular canal (ASC) is the most rounded of the semicircular canals in *Panthera leo* (Figs 2, S1). Only one of the juvenile *P. leo* (SMF 15765) features a slightly oval ASC (Fig. 2F). The posterior semicircular canal (PSC) is slightly more oval shaped than the ASC with varying degree between specimens (e.g., SMF 95010 and SMF 15765 in Fig. 2A, E). The lateral semicircular canal (LSC) is more oval than ASC and PSC and is slightly bent in posterolateral direction. However, there is some degree of variation in the shape of the LSC. Notably, the LSC of SMF 15765 (Fig. 2G) appears more oval than in all other lion specimens. In contrast,

the LSC in SMF 22104 (Fig. S1G) is the least oval within our sample. Even though undulating of the semicircular canals is minimal, there is some variation between the degrees of undulation between specimens. The highest degree of undulation can be found in the LSC followed by the ASC.

The ASC has the largest radius of curvature (R) amongst the three semicircular canals in all studied lion specimens (Table 2), albeit in SMF 22106 and SMF 1366 the PSC-R is only slightly smaller. The LSC has the smallest radius, except for SMF 22104, where the PSC has the smallest radius. In SMF 95010 the size difference between LSC and PSC is negligible. There is no notable difference in the radius between infant and adult specimens. Relative to skull length *P. leo* shows a negative allometry from SMF 95010 over SMF 15765 to the adult specimens (Fig. 3B, Table 2). Additionally, Figure 3B illustrates a decrease of the relative size differences between the three distinct semicircular canals, when standardized for skull basal length. However, this trend is not present when the radii are divided by inner ear height (Fig. S2A). Therefore, the increasing skull basal length reduces the effect of the relative size differences between the distinct semicircular canals.

Proportionally, the SCs of the neonate specimen (IDAS 1.1, SMF 95010) appear to be considerably thicker than the semicircular canals of the specimens in IDAS 1.2, 1.3 and 3 (Fig. 2). The neonate petrosal bone is still not fully ossified and denser bony material is surrounding the bony labyrinth; the older infant stages show increasing maturity of the petrosal bone (Fig. 4A–D).

The fossa subarcuata, whose entrance is limited by the ASC, is present in the neonate *P. leo* (IDAS 1.1, Figs 4A, 5A, E), but not in adult specimens (SMF 4643, Figs 4D, 5D, H). The infant SMF 15765 (IDAS 1.2, Figs 4B, 5B, F) and the infant SMF 38325 (IDAS 1.3, Figs 4C, 5C, G) show intermediate stages with partially closed fossa subarcuata, with the latter displaying an almost closed fossa subarcuata showing a distinct canal that might be the petromastoid canal. It is also apparent, that the bone density of the petrosal bone increases during ontogeny.

In all ontogenetic stages of *P. leo*, the ventral limb and the ampullae of the PSC and the posterior limb of the LSC are fused to form an osseous secondary crus commune. Although their spaces are confluent, the LSC and PSC are partly distinguishable since the lower limb of the PSC is on a lower level as the plane of the LSC, in anterior view (Figs 2A, E, I, M, S1A, E, I).

The ampullae of the semicircular canals, although not prominently inflated, are distinct. Right below the anterior and lateral ampulla there is a bony protuberance into the cavity of the bony labyrinth that is likely associated with the entrance of the anterior and lateral ampullar nerves (CN VIII) (Figs 2D, H, L, P, 6A, S1D, H, L). The bone of the protuberance has a lower density as the rest of the surrounding petrosal bone and there seems to be some degree of variation between the size and shape of this structure between specimens (Figs 2, 6A, S1).

The aquaeductus vestibuli leaves the vestibule anterior to the crus commune and runs medially. The proximal

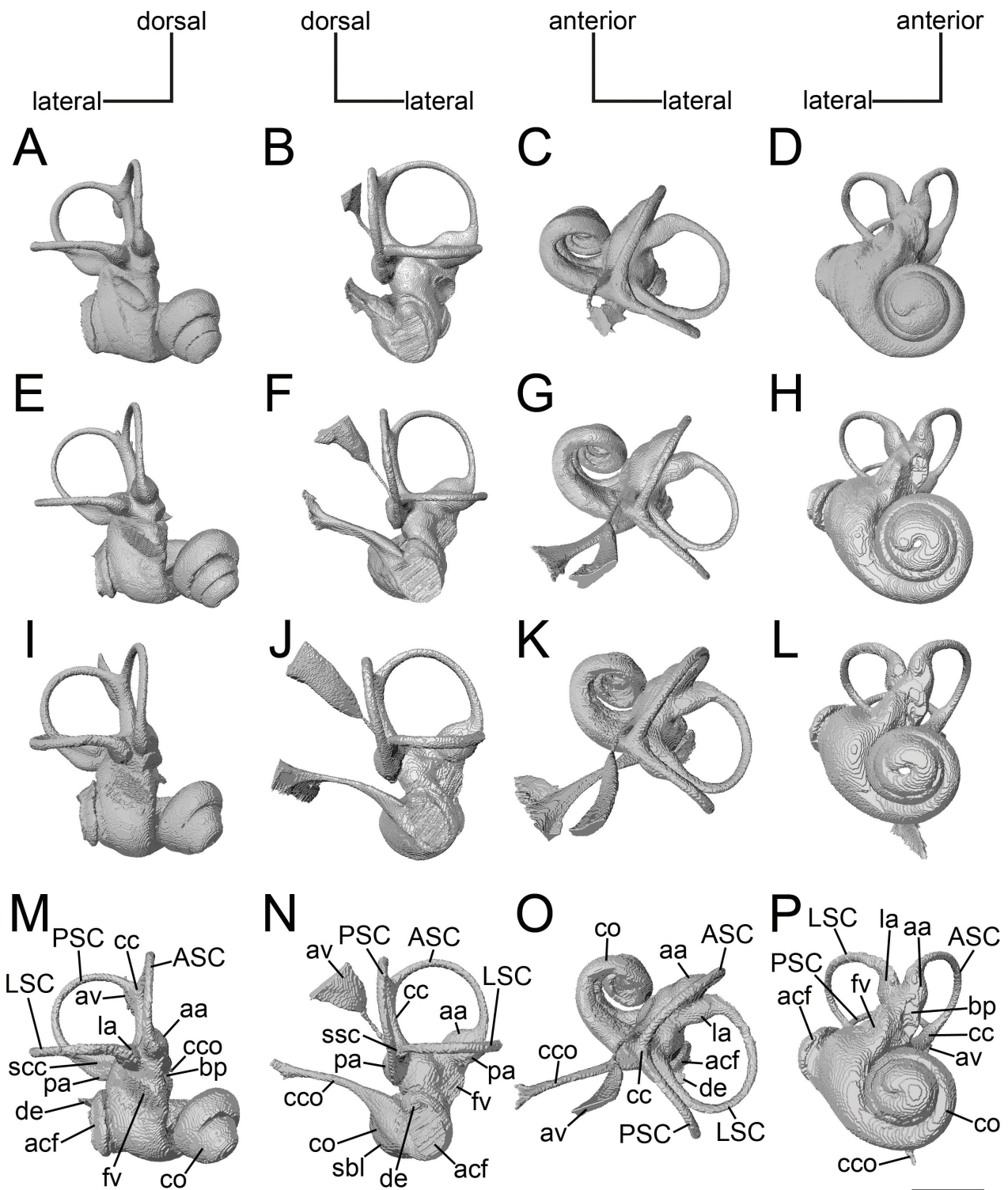


**Figure 2.** Virtual endocasts of the right bony labyrinth of *Panthera leo* represented by different ontogenetic stages. **A–D** SMF 95010, neonate (IDAS 1.1); **E–H** SMF 15765, infant (IDAS 1.2); **I–L** SMF 38325, infant (IDAS 1.3); **M–P** SMF 4643, adult (IDAS 3). Abbreviations: aa, anterior ampulla; acf, aperture of the cochlear fossula; ASC, anterior semicircular canal; av, aqueductus vestibuli; bp, bony protuberance; cc, crus commune; cco, canaliculus cochleae; co, cochlea; de, dorsal extension of the aperture of the cochlear fossula; fv, fenestra vestibuli; la, lateral ampulla; LSC, lateral semicircular canal; pa, posterior ampulla; PSC, posterior semicircular canal; sbl, secondary bony lamina; scc, secondary crus commune. Scale bar: 5 mm.

part is tubelike and increases in length with ongoing age, while the distal part fans out.

The fenestra vestibuli has an oval shape. The fenestra cochleae is hidden by the cochlear fossula and thus not visible in the endocasts as observed in other mammals

(e.g., Wible et al. 2009; Billet and Muizon 2013; Wible and Shelley 2020). The aperture of the cochlear fossula is oval and quite large. In case of SMF 15765 and SMF 4643 there is a dorsal extension of the aperture (Fig. 2I, M).

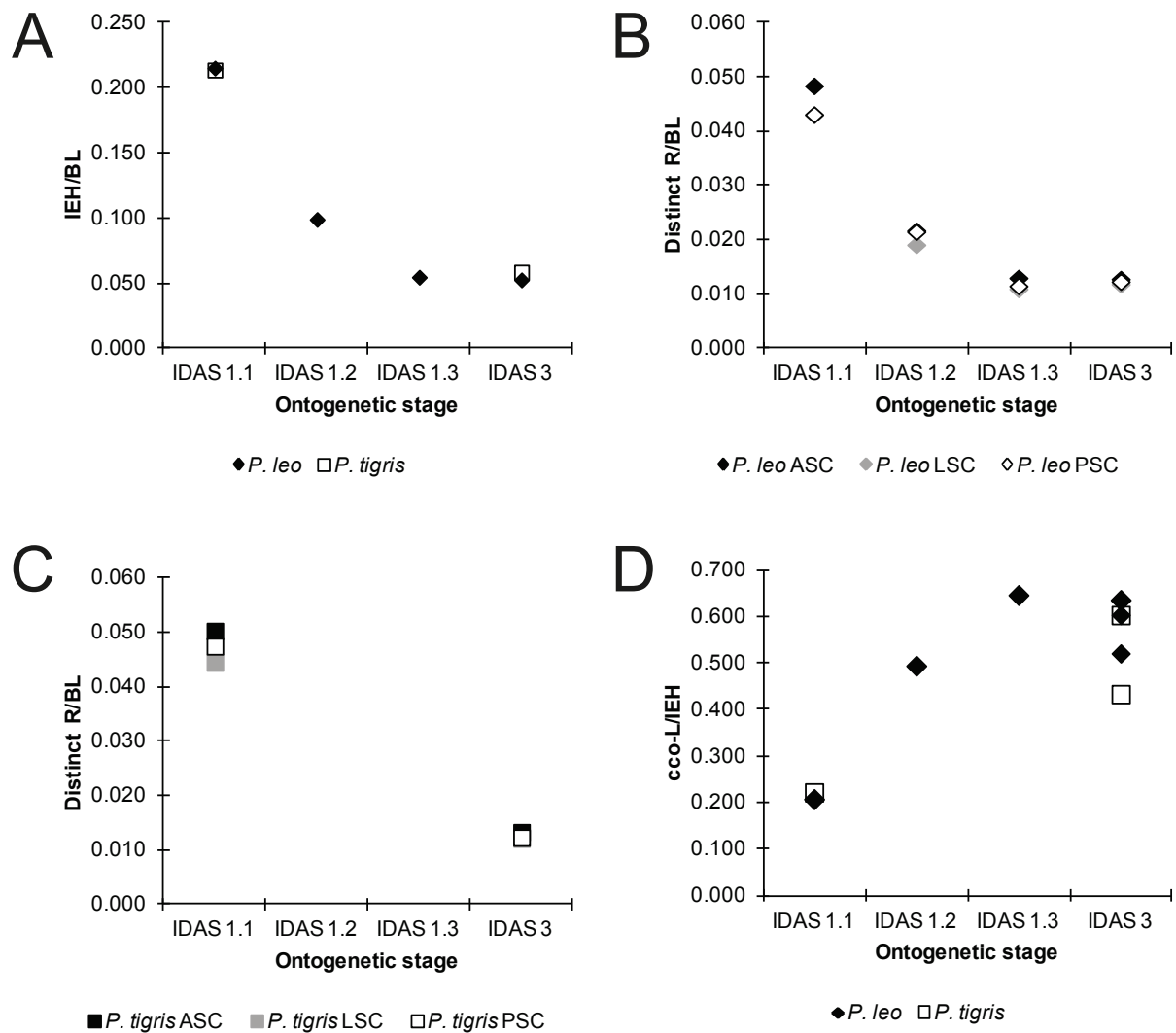


**Figure 3.** Ontogenetic transformations of selected structures and proportions in the bony labyrinth of *Panthera leo* and *P. tigris*. The y-axis refers to specific ratios, the x-axis refers to IDAS stages. Non-adult stages are represented by one specimen each, adult stages by four in *P. leo* and two in *P. tigris*; values of adult specimens are averaged (A–C). **A** Inner ear height against basal length in *P. leo* and *P. tigris*. **B** Size of the radius of curvature of the semicircular canals against basal length in *P. leo* (**B**) and *P. tigris* (**C**). **D** Elongation of the canaliculus cochleae during ontogeny in *P. leo* and *P. tigris*. Abbreviations: ASC, anterior semicircular canal; BL, skull basal length; cco-L, length of the canaliculus cochleae; IEH, inner ear height; LSC, lateral semicircular canal; PSC, posterior semicircular canal; R, radius of curvature.

In the adult specimens the canaliculus cochleae is a slightly curved, long bony canal, which first thins down in distal direction and then fans out (Figs 2N, O, S1B, C, F, G, J, K). However, the canaliculus cochleae of SMF 1366 is remarkable thicker than in the other adult *P. leo* (Fig. S1J, K). The size and shape of the canaliculus cochleae changes during ontogeny. The canaliculus cochleae of SMF 95010 (IDAS 1.1; Fig. 2B, C) is short and stout, whereas SMF 15765 (IDAS 1.2; Fig. 2F, G) shows an intermediate stage between SMF 95010 and the adult specimens. Albeit the canaliculus cochleae of SMF 1336 (IDAS 3; Fig. S1J, K) is in shape and proportion more similar to those of SMF 15765 (IDAS 1.2), while the one of SMF 38325 (IDAS 1.3; Fig. 2J, K) is more similar to the adult one. During ontogeny the canaliculus cochleae increases in length in absolute values and relative to IEH, while the petrosal bone increases in size around the inner ear (Figs 3D, 5, Table 2).

SMF 22101 (Fig. S1B, C) features a smaller canal extending from the distal part of the canaliculus cochleae, while in SMF 1366 (Fig. S1J, K) and SMF 38325 (Fig. 2J, K) the distal fanning is exceptionally large.

The cochlea forms a conical spiral. Except for SMF 22101, all cochlear spirals are sharply pointed (Table 2). The cochlea has three full turns in specimens of wild origin, except for SMF 4643 (Fig. 2P) which has 3.25 turns and SMF 22104 (Fig. S1H) which has 2.75 turns. The specimens of captive origin feature an additional quarter turn. One of the specimens of unknown origin features 3 turns (SMF 1366, Fig. S1L) and one 3.25 turns (SMF 38325, Fig. 2L). The mean length of the cochlea in *P. leo* is 48.818 (+/–1.850) mm. The cochlear length of the captive specimens is slightly longer than that of the wild ones (Table 2). The two specimens of unclear/unknown origin (SMF 1366 and SMF 38325) are in the range of captive specimens in our sample.

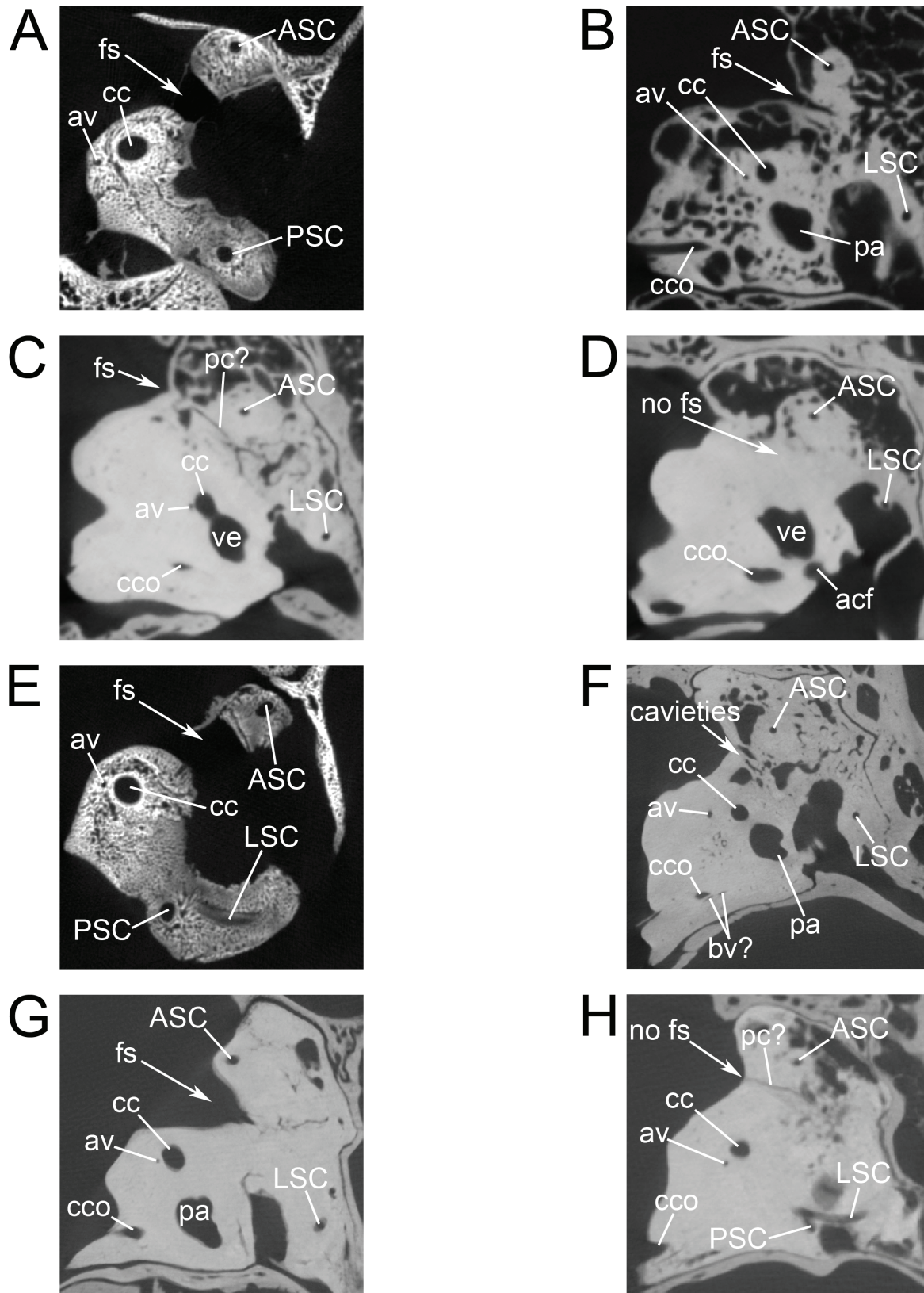


**Figure 4.**  $\mu$ CT images of the bony labyrinth in *Panthera* species showing selected structures and ontogenetic transformation of the fossa subarcuata. **A** neonate *P. leo* (SMF 95010, IDAS 1.1, right side, transversal), **B** infant *P. leo* (SMF 15765, IDAS 1.2, right side, transversal); **C** infant *P. leo* (SMF 38325, IDAS 1.3, right side, transversal); **D** adult *P. leo* (SMF 4643, right side, oblique transversal); **E** neonate *P. tigris* (SMF 15722, IDAS 1.1, left side mirrored, transversal); **F** adult *P. tigris* (SMF 15737, right side, transversal); **G** infant *P. pardus* (SMF 15745, IDAS 1.2, left side mirrored, transversal); **H** adult *P. pardus* (SMF 94342, IDAS 3, right side, transversal). Abbreviations: aa, anterior ampulla; acf, aperture of the cochlear fossula; ASC, anterior semicircular canal; av, aqueductus vestibuli; bv, canal for blood vessels; cc, crus commune; cco, canaliculus cochleae; fs, fossa subarcuata; la, lateral ampulla; LSC, lateral semicircular canal; pa, posterior ampulla; pc, petromastoid canal; PSC, posterior semicircular canal; scc, secondary crus commune; ve, vestibule. Not to scale.

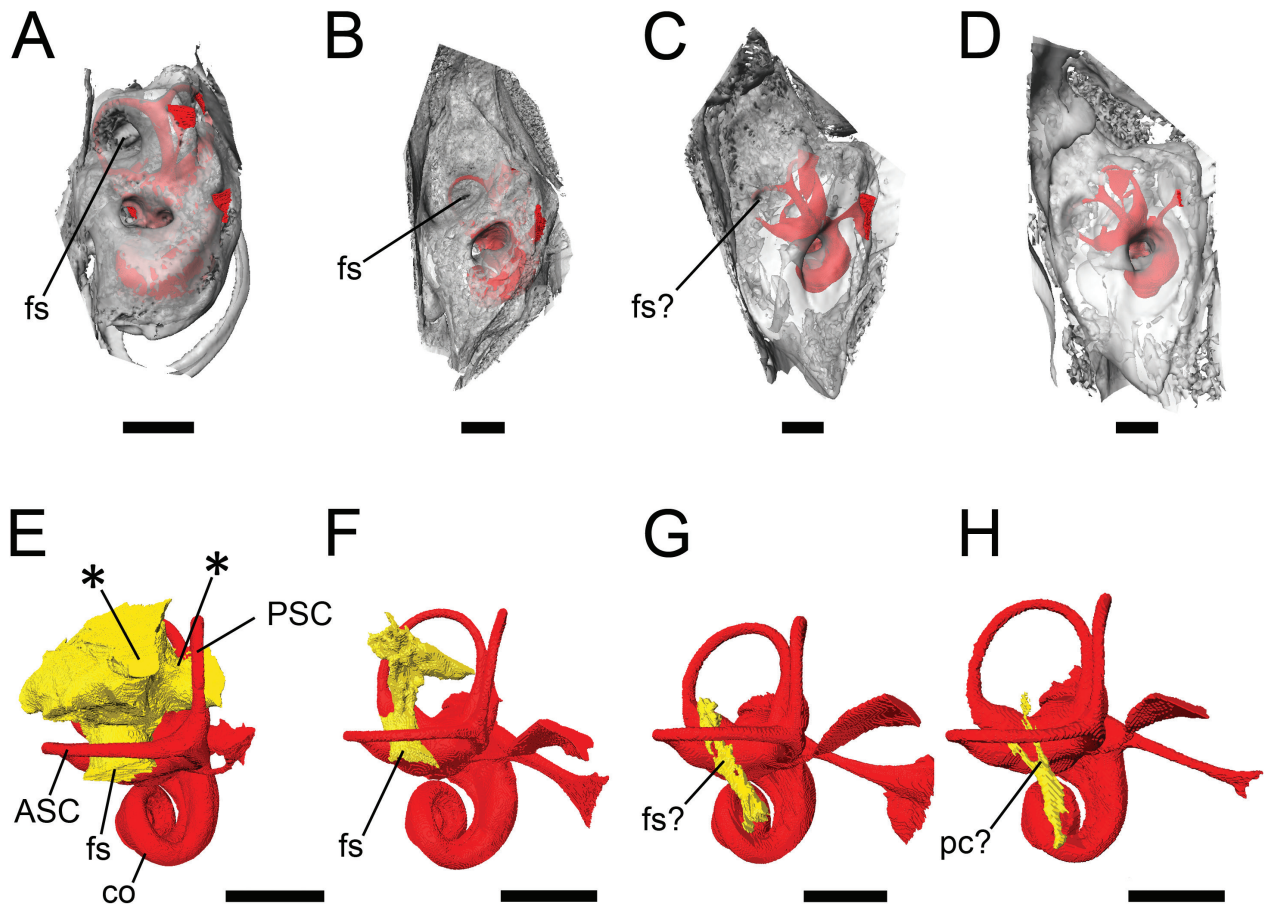


**Figure 5.** Virtual 3D models of the right bony labyrinth (red), petrosal bone (grey) and fossa subarcuata (yellow) of *Panthera leo* revealing ontogenetic changes of size proportions. **A–D** in dorsomedial view, posterolateral margin to the top and **E–G** in dorsal view, posterolateral to the top. **A, E** SMF 95010, neonate (IDAS 1.1); **B, F** SMF 15765, juvenile (IDAS 1.2); **C, G** SMF 38325, juvenile (IDAS 1.3); **D, H** SMF 4643, adult (IDAS 3). Abbreviation: ASC, anterior semicircular canal; co, cochlea; fs, fossa subarcuata; pc, petromastoid canal; PSC, posterior semicircular canal; asterisks (\*) refer to unspecified connected cavities. Scale bars: 5 mm.

The secondary bony lamina is not or only partly visible in some specimens ( $\mu$ CT slides and digital endocasts), maybe due to scan resolution. In most specimens the secondary bony lamina is traceable close to half a turn of the cochlea and in SMF 95010 half a turn of the cochlea. In SMF 220104 and SMF 38325 it is only visible for one third of a turn and not visible in SMF 1366 (Table 2).

### Comparison with further *Panthera* species

Generally, bony labyrinth morphology of the other *Panthera* species resembles the patterns observed in *P. leo* (Figs 7, 8, S3). Main differences can be observed in size and proportions of the semicircular canals, the presence of an osseous secondary crus commune and the number of cochlear turns. However, *P. pardus* deviates in many respects from the other species.

When corrected for skull basal length, the larger species (*P. leo*, *P. tigris*) have slightly smaller IEH, and thus relatively smaller bony labyrinths, than the smaller species (*P. pardus*, *P. onca*, *P. uncia*) (Fig. 9A, Table 2). In the available measurements *P. tigris* and *P. pardus* shows

a negative allometry of the inner ear with the surrounding petrosal during ontogeny (Fig. 3, Table 2).

The shape of the semicircular canal curvature varies from round to oval and shows some variation in those species represented by more than one specimen. This is especially the case in *P. tigris* (Fig. 7M–T). As in *P. leo* the ASC is round in *P. pardus*, *P. tigris*, *P. uncia* (Figs 7, 8). In contrast *P. onca* shows an oval or slightly D-shaped ASC (Fig. 8B). The LSC is round to slightly oval in *P. pardus* (in SMF 94342 significantly oval, Fig. S3C), D-shaped in *P. uncia* (Fig. 8G), and – as in *P. leo* – oval in *P. onca* and *P. tigris* (Figs 7O, S, 8C, S3G, K). The PSC of *P. pardus*, *P. onca*, and *P. tigris* is oval, whereas in *P. uncia* it is round (Figs 7A, E, I, M, Q, 8A, E, I, M, S3A, E, I).

Slight undulation of the semicircular canals can also be observed in other *Panthera* species, whereas *P. uncia* shows the highest degree of undulation in our sample. As in *P. leo* the ASC shows the largest radius of curvature in all other *Panthera* species followed by the PSC and the LSC, except for *P. tigris* SMF 15737 (Table 2). However, in some specimens the size difference between LSC and PSC is minor. In contrast to *P. leo*, *P. pardus*, *P. onca*, and *Neofelis* spp. the LSC of *P. uncia* and the LSC of all but one *P. tigris* (SMF 7020) projects further laterally than the PSC (Figs 8G, S3K).

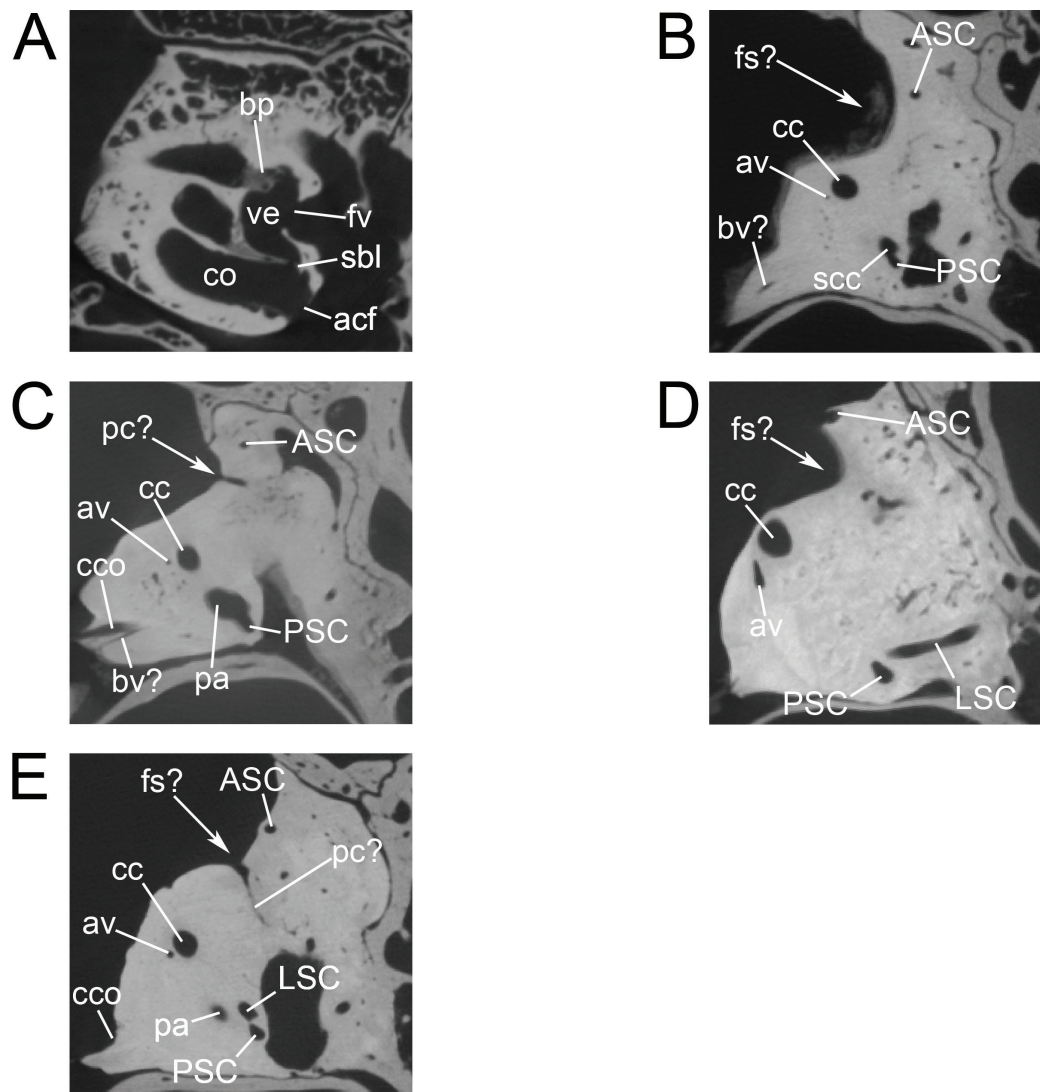


**Figure 6.**  $\mu$ CT images of the bony labyrinth in Pantherinae showing the bony protuberance that transmits branches of the nervus vestibulocochlearis (CN VIII) and patterns of the fossa subarcuata. **A** infant *Panthera leo* (SMF 15765, IDAS 1.2, right side, transversal); **B** *P. onca* (SMF 3067, right side, transversal); **C** *P. uncia* (SMF 5419, left side mirrored, transversal); **D** *Neofelis diardi* (SMF 15470, left side mirrored, transversal), the ASC is not completely enclosed by the petrosal bone; **E** *N. nebulosa* (SMF 40850, right side, transversal). Abbreviations: acf, aperture of the cochlear fossula; ASC, anterior semicircular canal; av, aquaeductus vestibuli; bp, bony protuberance; bv, canal for blood vessels; cc, crus commune; co, cochlea; fs, fossa subarcuata; fv, fenestra vestibuli; LSC, lateral semicircular canal; pa, posterior ampulla; pc, petromastoid canal; PSC, posterior semicircular canal; sbl, secondary bony lamina; scc, secondary crus commune; ve, vestibule. Not to scale.

Figure 9A illustrates negative allometry of the IEH with the skull basal length when comparing adult specimens of different pantherine species. Therefore, smaller species have a proportional larger inner ear relative to skull basal length as larger species. One notable exception, however, is *P. onca*, which is heavier than *P. pardus* and *P. uncia*, but has a relatively larger inner ear. However, the semicircular canal radii are relatively smaller than in *P. uncia* and of comparable size or smaller than in *P. pardus* (Fig. 9 A–E).

Concerning ontogeny, semicircular canal radii are proportionally larger in the neonate *P. tigris* than in the adult which resembles the negative allometric pattern as observed in *P. leo* (Fig. 3B, C, Table 2). As in *P. leo*, the relative size differences of the three semicircular canals of *P. tigris* decrease during ontogeny; however, this is

caused by the increasing skull basal length and no pattern is apparent in *P. tigris* and *P. pardus* when standardized for inner ear height (Fig. S2B, C). The petrosal bone of the neonate *P. tigris* shows the same ossification pattern and level of maturity like the neonate lion and the juvenile *P. pardus* (IDAS 1.2) resembles the IDAS1.3 stage in *P. leo* (Fig. 4). Interestingly, Figure 9C–E illustrates different patterns of intraspecific variation in semicircular canal radii between *Panthera* species. While there is only little variation in the radius of curvature of ASC and PSC relative to skull basal length, the LSC varies the most in *P. leo*. However, *P. pardus* shows the opposite pattern and in *P. tigris* the PSC-R reveals the highest variation. All in all, the semicircular canal radii of *P. tigris* vary less than in the other species relative to skull basal length.

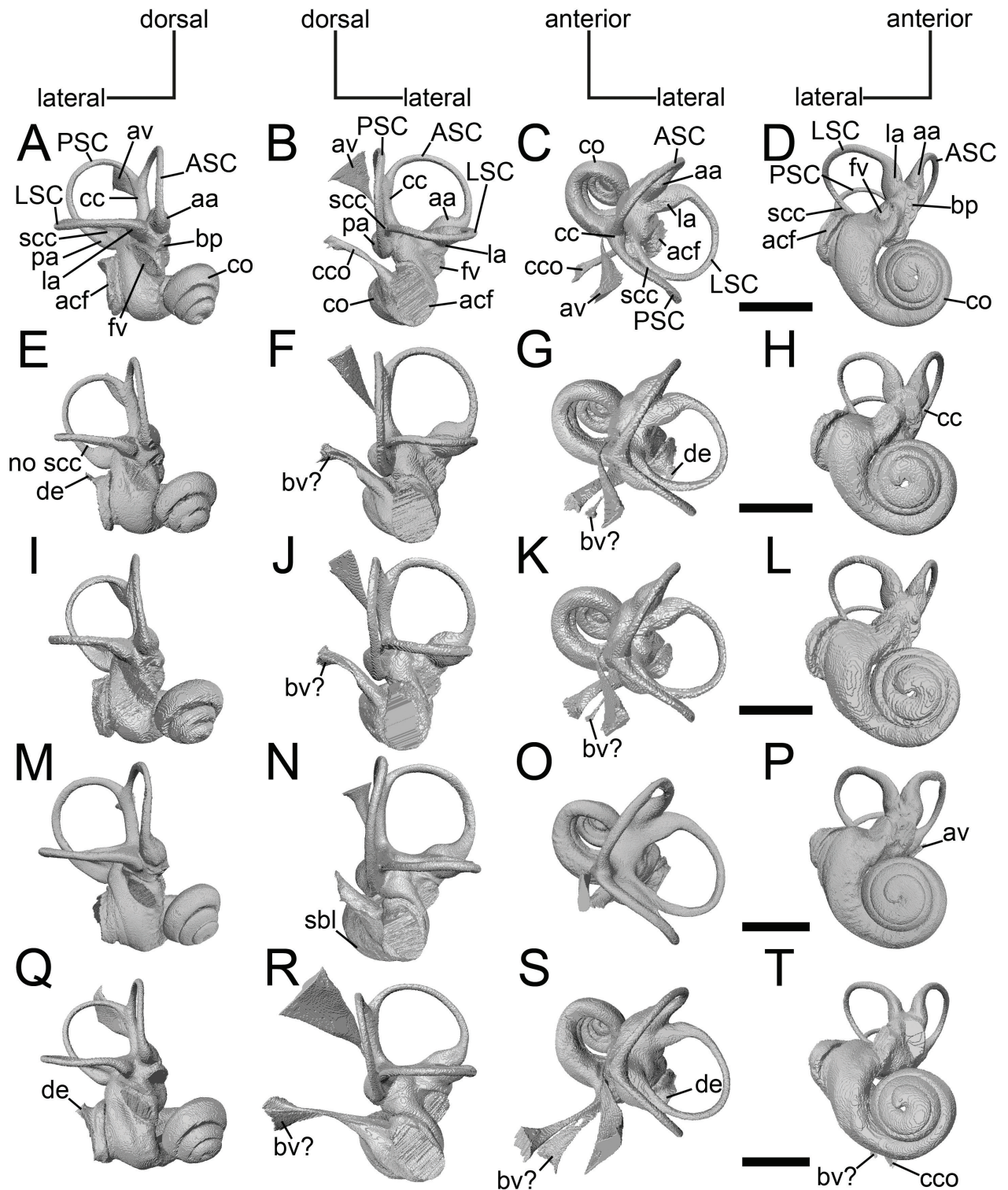


**Figure 7.** Virtual endocasts of the right bony labyrinth of selected *Panthera* species represented by different ontogenetic stages. A–D infant *P. pardus* (SMF 15745, left side mirrored); E–H adult *P. pardus* (SMF 16259); I–L adult *P. pardus* (SMF 16259, left side mirrored); M–P neonate *P. tigris* (SMF 15722, left side mirrored); Q–T adult *P. tigris* (SMF 15737). Abbreviations: aa, anterior ampulla; acf, aperture of the cochlear fossula; ASC, anterior semicircular canal; av, aquaeductus vestibuli; bp, bony protuberance; bv, canal for blood vessels; cc, crus commune; cco, canaliculus cochleae; co, cochlea; de, dorsal extension of the aperture of the cochlear fossula; fv, fenestra vestibuli; la, lateral ampulla; LSC, lateral semicircular canal; pa, posterior ampulla; PSC, posterior semicircular canal; sbl, secondary bony lamina; scc, secondary crus commune. Scale bars: 5 mm.

The adult specimens of the studied *Panthera* species do not have a fossa subarcuata, but the infant specimens show its ontogenetic transformation (Figs 4–6). Similar to *P. leo*, the neonate *P. tigris* (IDAS 1.1) has a distinct

fossa subarcuata (Fig. 4E). In contrast, the fossa of the infant *P. pardus* (also IDAS 1.2) is already in the process of being closed by the petrosal bone, displaying a deep funnel-shaped depression (Fig. 4G). Interestingly, the

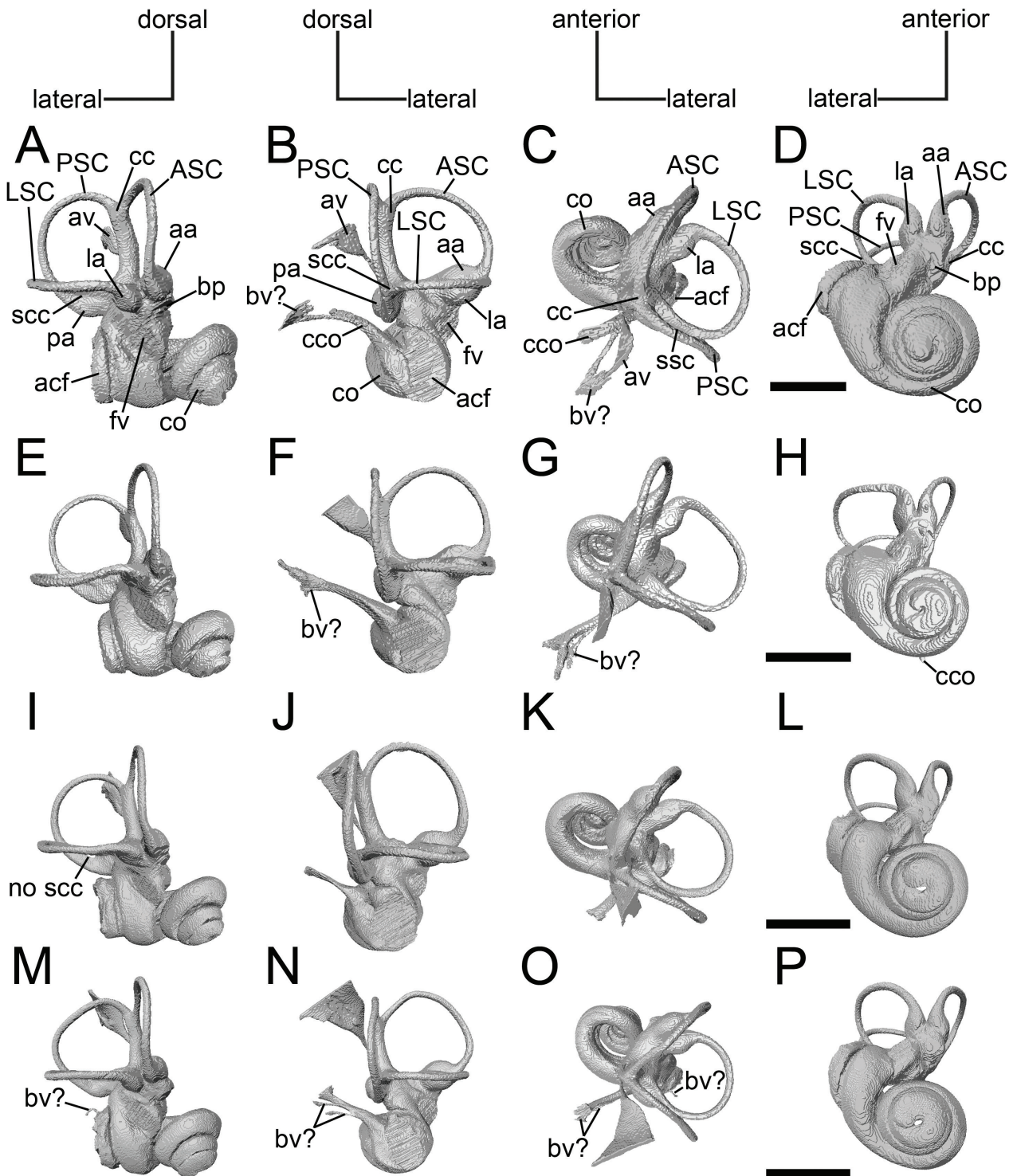


**Figure 8.** Virtual endocasts of the right bony labyrinth of selected adult Pantherinae. **A–D** *Panthera onca* (SMF 3067); **E–H** *P. uncia* (SMF 5419, left side mirrored); **I–L** *Neofelis diardi* (SMF 15470, left side mirrored); **M–P** *N. nebulosa* (SMF 40850). Abbreviations: aa, anterior ampulla; acf, aperture of the cochlear fossula; ASC, anterior semicircular canal; av, aquaeductus vestibuli; bp, bony protuberance; bv, canal for blood vessels; cc, crus commune; cco, canaliculus cochleae; co, cochlea; fv, fenestra vestibuli; la, lateral ampulla; LSC, lateral semicircular canal; pa, posterior ampulla; PSC, posterior semicircular canal; sbl, secondary bony lamina; scc, secondary crus commune. Scale bars: 5 mm.

adult *P. pardus* (SMF 16529) and *P. onca* show on both sides a distinct concavity in the petrosal bone where the fossa subarcuata would be located (Fig. 6B). One adult *P. tigris* (SMF 15737) has a closed fossa subarcuata, but a high number of small cavities in this area (Fig. 4F). The adult *P. pardus* specimens show a narrow canal in the area

of the former fossa subarcuata that might represent the petromastoid canal (Fig. 4H). *Panthera uncia* shows a slight depression and presumably a relatively broad petromastoid canal or a closing fossa subarcuata (Fig. 6C).

The osseous secondary crus commune is present in all *Panthera* species (Figs 7, 8, S1, S3, S4). However, it is

relatively shorter in *P. leo* and *P. uncia* than in *P. pardus* and *P. onca* and shortest in *P. tigris* (Fig. S4). In addition, two specimens of *P. pardus* deviate from this pattern in lacking the osseous secondary crus commune on the left side (SMF 16259) and on both sides (SMF 94342), respectively (Fig. 7I, M, S3A, E).

As in *P. leo*, the ampullae in the other *Panthera* species are distinct, but not significantly inflated. They appear to be proportionally larger in the smaller species (i. e., *P. pardus*, *P. onca*, *P. uncia*, Figs 7A–L, 8A–H, S3A–H), than in the larger ones (i.e., *P. leo*, *P. tigris*, Figs 2, 7M–T, S1, S3I–L). The bony protuberance into the vestibule below the anterior and lateral ampulla is also present in the other studied *Panthera* specimens but is very irregular in shape (Figs 7D, H, L, P, T, 8D, H, S3D, H, L).

In all *Panthera* species, the aquaeductus vestibuli runs medially, leaving the vestibule anterior to the crus commune. Size and proportions of the proximal thin part and the distal fanning out part vary between species and individuals. Additionally, the angle of the fanning differs between individuals (Figs 7B, F, J, N, R, 8B, F, S3B, F, J). It is least pronounced in *P. pardus* (Figs 8A–L, S3A–H). While in the other *Panthera* species there is a distinct transition between proximal and distal part, in *P. pardus* the transition is much smoother. As in *P. leo*, in the infant *P. pardus* the proximal part of the aquaeductus vestibuli is proportionally longer than the distal part. However, this pattern is not present in the neonate *P. tigris* (Fig. 7N, O).

Both, the fenestra vestibuli and the aperture of the cochlear fossula are oval in all *Panthera* specimens (Figs 7, 8, S3). Like in *P. leo* the right bony labyrinth of *P. pardus* SMF 16259 and *P. tigris* SMF 15737 show a dorsal extension of the aperture of the cochlear fossula (Fig. 7E, Q).

The canaliculus cochleae of adult stages of *P. pardus* and *P. tigris* is slightly curved with thinning in the middle section (Figs 7, 8, S3). The neonate *P. tigris* (Fig. 7N, O) has a short and stout canaliculus cochleae that, relative to IEH and in absolute values, increases (Table 2). The canaliculus cochleae of *P. tigris* increases in length during ontogeny as observed in *P. leo* (Fig. 3D, Table 2). The shape and proportions in *P. pardus* are similar to the IDAS 1.2 stage of *P. leo*, except for specimen SMF 94342, whose canaliculus cochleae is more similar to the one of adult lions.

In comparison to the canaliculus cochleae of adult *P. leo* specimens the canaliculus cochleae of *P. onca* is proportionally shorter with a more consistent diameter and is not fanning out distally (Fig. 8B, C). Considering the short skull basal length of *P. uncia*, the canaliculus cochleae is proportionally longer than in the other *Panthera* species and also shows thinning in the middle section (Fig. 8F, G). Small canals (labeled “bv” in Figs 7, 8) that branch off along the canaliculus cochleae are present in *P. pardus* (SMF 16259, Fig. 7G, K), *P. tigris* (SMF 15737, Fig. 7S), *P. uncia* (Fig. 8B, C) and *P. onca* (Fig. 8G).

The cochlea is conical spiral in all non-lion *Panthera* specimens and the number of cochlear turns ranges from 3 to 3.5 (Figs 7, 8, S3, Table 2). In *P. pardus*, the cochlea of captive individuals (SMF 94342, SMF 95992, Fig. S3) has 3 full turns, while that of SMF 16259 has 3.25 turns

and SMF 15745 shows 3.5 turns. In *P. tigris* the cochlear turn number ranges from 3 (SMF 15737, SMF 7020, Fig. S3) up to 3.25 (SMF 15722). The cochlea of *P. onca* has almost 3.5 turns, while the cochlea of *P. uncia* shows 3 turns (Fig. 8).

After correction for skull basal length, cochlear length is similar between specimens of the same species (Table 2, Fig. 9B). In addition, the bigger sized species (*P. leo* and *P. tigris*) can be distinguished from the smaller ones (*P. pardus*, *P. onca*, *P. uncia*). In case of the latter, the inner ear is, in relation to the skull basal length, larger than in the former, when excluding IDAS 1. *Panthera uncia* has the shortest cochlea in the entire sample in absolute values (Table 2). Again, as in *P. leo* ontogenetic stages of *P. tigris* and *P. pardus* (at least for the available measurements) reveal negative allometry of the size of the radii of all three semicircular canals as well as the canaliculus cochleae with the inner ear height and skull basal length (Table 2). The same holds true for comparing inner ear height with skull basal length (Fig. 3A, C, D).

*Panthera onca*, *P. pardus* (SMF 15745, right bony labyrinth of SMF 16259), and *P. tigris* (SMF 15737) show a traceable secondary bony lamina, close to half a turn of the cochlea. In another *P. tigris* specimen (SMF 15722) the secondary bony lamina reaches over half a turn. No secondary bony lamina is visible in all other specimens (Table 2).

## Comparison with *Neofelis* spp.

The inner ear morphology of *Neofelis* resembles those observed in *Panthera* (Fig. 8I–P). The main differences are the shape and proportions of the semicircular canals and, with the exception of certain *P. pardus* specimens, absence of the osseous secondary crus commune.

In absolute values, *N. nebulosa* has the smallest IEH and *N. diardi* the second smallest. Corrected for skull basal length, *N. diardi* has a proportionally larger bony labyrinth than *N. nebulosa*, representing the size proportion in IDAS 1.2 stage of *P. leo* (Fig. 9, Table 2). In contrast, *N. nebulosa* is closer in size to the adult *P. onca* (SMF 3067) and *P. uncia* (SMF 5419).

Furthermore, the index IEH/BL of both *Neofelis* species is greater than in the adult *Panthera* specimens, with the highest value (0.090) in *N. diardi* (Table 2). This pattern refers to negative allometry of the bony labyrinth with the skull basal length.

In *N. diardi* the curvature of the ASC is oval, the LSC and PSC are almost round (Fig. 8J). The ASC protrudes out of the petrosal bone because it is not entirely covered by bony material (Fig. 6D). The ASC and PSC of *N. nebulosa* are angular and the LSC is round (Fig. 8M–O). In both *Neofelis* species, the semicircular canals are slightly undulating and the ASC has the largest radius of curvature, while the LSC has the smallest (Table 2).

Overall, *N. diardi* has the largest inner ear in relation to body weight and skull basal length of all studied Pantherinae (Fig. 9). *Neofelis* spp. have proportionally larger cochlear sizes as well as larger SCs, with one notable

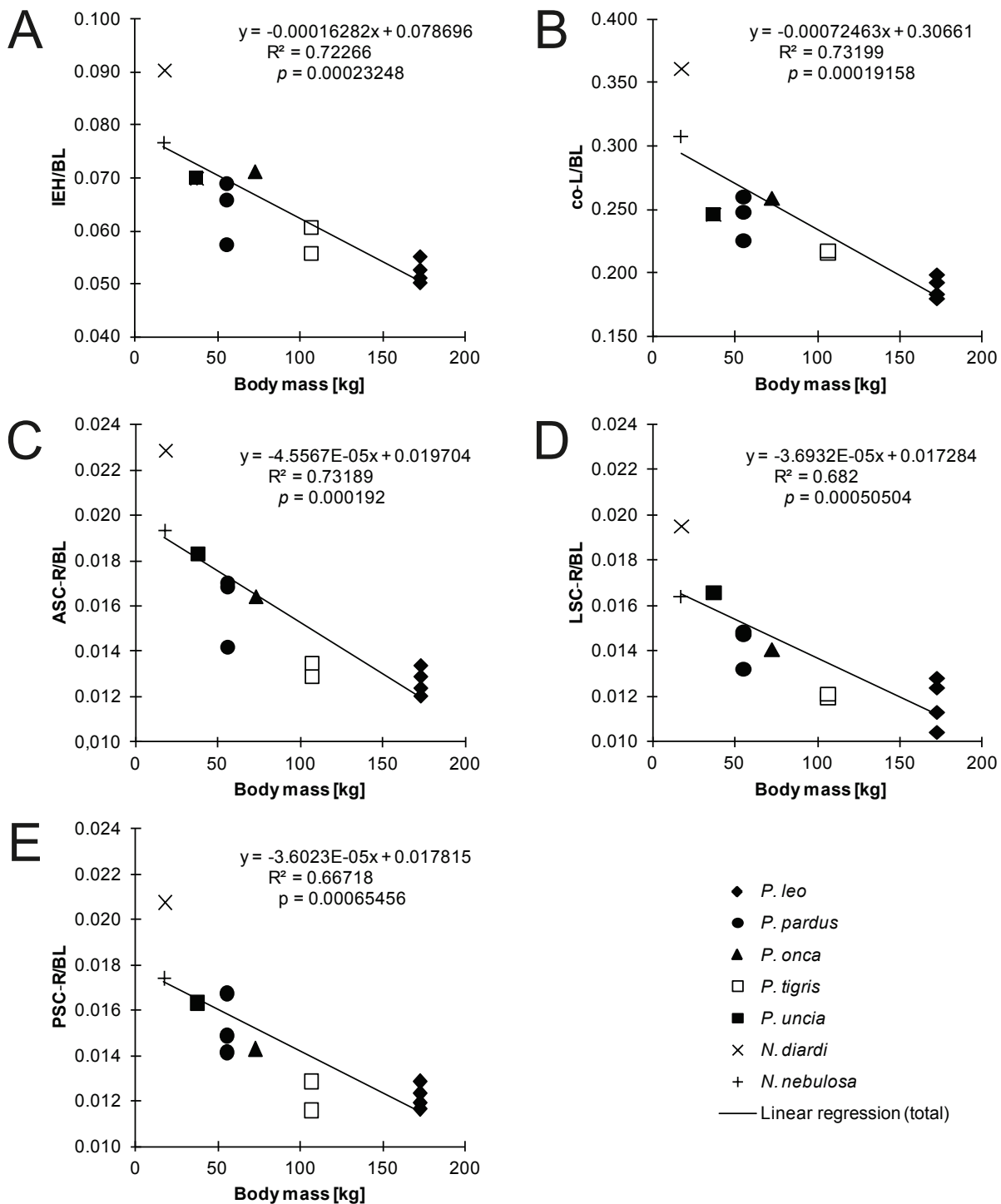


**Figure 9.** Size comparison of selected structures standardized by basal length in adult stages of all studied Pantherinae species. The values of species represented by multiple specimens are averaged. The linear equation, the coefficient of determination ( $R^2$ ) and the  $p$ -value are given in the respective graph. **A** inner ear height, **B** cochlear length, **C** anterior semicircular canal radius of curvature, **D** lateral semicircular canal radius of curvature, **E** posterior semicircular canal radius of curvature. Abbreviations: ASC, anterior semicircular canal; BL, skull basal length; co-L, cochlear length; IEH, inner ear height; LSC, lateral semicircular canal; PSC, posterior semicircular canal; R, radius of curvature.

exception. The LSC of *P. uncia* is proportionally larger than in *N. nebulosa* (Fig. 9). When standardizing for IEH and not skull basal length, the patterns are different (Fig. S5). The values of the two *Neofelis* species are almost congruent, while the range of values in *P. leo* dramatically increases, which is also true for *P. tigris*. In case of the LSC, the range of *P. leo* is larger than in *P. pardus*.

The semicircular canal radii of *P. onca* and *P. tigris* are distinctly below average.

In the area of the fossa subarcuata in *N. nebulosa* a concavity similar to that in *P. onca* is present, albeit not as pronounced as in the latter. In contrast, *N. diardi* shows a shallow funnel-shaped depression in the area that we interpret as a remnant of the fossa subarcuata, which tran-

sitions into a possible petromastoid canal. However, the density of the surrounding bone as well as the adult age do not indicate any further closing of both cavities (Fig. 6D, E).

Like in the studied *Panthera* specimens, in anterior view, the lower limb of the PSC is on a lower level as the plane of the LSC but both *Neofelis* species lack an osseous secondary crus commune (Fig. 8I, M). Like in *Panthera*, the ampullae of the SCs are distinct, but not remarkably inflated in both *Neofelis* species (Fig. 8I–P). Proportionally, they appear in size more similar to the small *Panthera* species (i.e., *P. pardus*, *P. onca*, *P. uncia*). Both *Neofelis* species reveal the bony protuberance below the anterior and lateral ampulla observed in *Panthera*. *N. nebulosa* shows a distinct canal in this structure (Fig. 8L, P). Shape and course of the aquaeductus vestibuli of *Neofelis* resembles the pattern observed in adult *Panthera* specimens (Fig. 8J, N).

Just like in *Panthera*, the fenestra vestibuli and the aperture of the cochlear fossula are oval in both *Neofelis* species. However, in *N. nebulosa*, a small canal is branching off from the dorsal edge of the aperture of the cochlear fossula (Fig. 8M).

The canaliculus cochleae of *N. diardi* resembles mostly the pattern in *P. onca* whereas that of *N. nebulosa* is fanning out distally, but not as much as in adult *P. leo* or *P. tigris* (Fig. 8J–K). In *N. nebulosa* two small canals branch off in the middle section (Fig. 8N).

The cochlea is conical spiral in all *Neofelis* specimens. The number of turns in *N. diardi* is 3, while in *N. nebulosa*, the number of turns is 3.25 (Fig. 8L, P).

Albeit, smaller in skull basal length, both *Neofelis* species have, in absolute values, a longer cochlea as *P. uncia*, but shorter than the other adult *Panthera* specimens (Table 2); *N. diardi* has a cochlear length similar to that of the infant *P. pardus*. However, corrected for skull basal length, *N. diardi* has the longest and *N. nebulosa* has the second longest cochlea of the adult Pantherinae sample (Fig. 9B, Table 2). In *N. diardi* the secondary bony lamina reaches close to half a turn of the cochlea, while in *N. nebulosa* it reaches close to three quarter of a turn (Table 2).

## Discussion

### Systematic and morphofunctional implications

The ASC has the largest radius of curvature in our sample, as it is typical for mammals (e.g., Ekdale 2013). Among Carnivora the aquatic *Eumetopias jubatus* is the only known exception to this rule in that the LSC has the largest radius of curvature (Ekdale 2013).

Overall, the bony labyrinth morphology is very similar between Pantherinae specimens, although species can be distinguished by certain features. The shape of the semicircular canals can be used to distinguish the genera *Pan-*

*thera* and *Neofelis*. This is most prominent in the ASC, as it is round in almost all *Panthera* specimens and oval (*N. diardi*) or angular (*N. nebulosa*) in *Nebulosa*.

Within *Panthera*, *P. leo* and *P. tigris* can be distinguished by the length of the osseous secondary crus commune, which is relatively short in the latter. Additionally, in contrast to *P. leo*, the LSC of most *P. tigris* specimens protrudes the PSC. *Panthera uncia* is easily identifiable by the shape of the LSC and the relatively large semicircular canals. The latter indicate a good sense of balance, which is crucial for a mountain dwelling species for locomotion in rocky terrain (e.g., Wilson and Mittermaier 2009). *Panthera onca* is recognizable by its D-shaped ASC. Living in vastly different environments, the relatively short cochlea of *P. uncia* (mountain terrain) and the relative long cochlea of *P. onca* (forested areas) is an interesting aspect, which should be investigated in the future, as the morphology of the cochlea has a direct effect on hearing abilities (Wilson and Mittermaier 2009; Ekdale 2016). Using the relative length of the canaliculus cochleae, it is also possible to distinguish *P. pardus* from *P. leo* in adult specimens, which is the result of the difference in overall size of the petrosal bone.

The presence or absence of the small branching canals of the canaliculus cochleae cannot be used for identifying the distinct species. It is tempting to assume that these delicate canals are only visible in the specimens whose scans have a higher resolution. However, the infant *P. leo* (SMF 95010) has been scanned with higher resolution than the other *P. leo* specimens and does not feature these small canals. In addition, the infant *P. tigris* (SMF 15722) does not feature them either, while one of the adult tigers (SMF 15737) does. Whether this is intraspecific and/or ontogenetic variation and/or caused by the quality of the scan needs to be elucidated in future studies.

As shown in former studies on different taxa, the larger species have a relatively smaller bony labyrinth than the smaller species, even though, the absolute size does not vary much in case of Pantherinae (e.g., Spoor et al. 2007; Ekdale 2013; Costeur et al. 2019). However, in our opinion, the IEH of *P. uncia* does not represent the overall bony labyrinth size very well, because of its large semicircular canals. It is remarkable, that *N. diardi* and *N. nebulosa*, although almost equal in body size, differ greatly in terms of semicircular canal and cochlear size proportions (Fig. 9). Hence, a functional reason for these differences is likely and regarding SC-R, traditionally it might be expected, that *N. diardi* is more agile than *N. nebulosa* (Spoor et al. 2007). Due to their secretive way of life, not much is known about the ecology of wild *Neofelis* species and most information are obtained from captive animals, which do not concur with the rare wild sightings (Hemmer 1968; Sunquist and Sunquist 2002 and references therein). In addition, most of these observations were obtained before the two species were separated (Buckley-Beason et al. 2006; Kitchener et al. 2006). A closer examination of the ecology for both species could help to elucidate functional adaptations in the inner ear.

Furthermore, the phylogenetic or ecological implications for the different relative sizes of the semicircular

canals in Pantherinae species, should be recorded in larger sample sizes and complemented by additional morphometric measurements and statistically evaluated as described by Schwab et al. (2019). We also suggest, that with recent developments in Pantherinae phylogeny and taxonomy (e.g., Buckley-Beason et al. 2006; Kitchener et al. 2006; Kitchener et al. 2017), future studies on the ecology of Pantherinae species should be conducted to improve our understanding of different populations. These data can help to reveal morphological differences among populations and therefore contribute to taxonomic revisions on the subspecies level.

Among the Felidae studied by Etmayr (2014), *Puma concolor* (fig. 39) is most similar to *Panthera*; the canaliculus cochleae is relatively short and comparable to *P. pardus* or the oldest infant *P. leo* (IDAS 1.3). All semicircular canals of *Caracal caracal* are oval and the cochlea appears to have a higher aspect ratio than observed in our *P. leo* sample (Etmayr 2014, fig. 40). With its relatively large semicircular canals and missing osseous secondary crus commune, *Acinonyx jubatus* (Grohé et al. 2018) can be easily distinguished from Pantherinae.

Concerning the osseous secondary crus commune, our findings are similar to data from literature. Hyrtl (1945) describes an osseous secondary crus commune in *P. leo*, *P. tigris* and *P. pardus*. Of the four *P. pardus* specimens in our sample, two have an osseous secondary crus commune on both sides, one on the right side and one on neither side, which implicates some intraspecific variation. There is no consistency in the order Carnivora regarding presence or absence of an osseous secondary crus commune. Ekdale (2013) argued that relative to the ampullar entrance of the PSC, high positioned LSC is the plesiomorphic condition for Carnivora, while a low positioned LSC is a synapomorphy for Caniformia. The latter character state can refer to presence of an osseous secondary crus commune as observed in *Canis lupus* and *C. lupus familiaris* (Ekdale 2013; Schwab et al. 2019, fig. 1). Thus, presence of an osseous secondary crus commune has to be regarded as a derived character within Carnivora. However, *Eumetopias jubatus* lacks an osseous secondary crus commune (Ekdale 2013).

Among Felidae, *Neofelis* spp., *Acinonyx jubatus* and *Caracal caracal* lack an osseous secondary crus commune (Etmayr 2014, fig. 40; Grohé et al. 2018, fig. 2). Given Ekdale's (2013) character polarization this would represent the plesiomorphic carnivoran grundplan. In contrast *Panthera* spp. and other Felinae that have an osseous secondary crus commune represent a derived pattern. Etmayr (2014) reported an osseous secondary crus commune for *Felis chaus*; the author was not sure in case of *Prionailurus viverrinus*. However, its bony labyrinth endocast in figure 41 appears to show one. The same holds true in the case of *Puma concolor* (fig. 39), although no information is given in the text. Intraspecific variation as observed in our *P. pardus* sample, does also occur in *Felis catus* as different studies report the absence as well as presence of an osseous secondary crus commune (Ekdale 2013; Schellhorn 2018). Albeit, the sample of *Felis catus* specimens in Schellhorn (2018) is larger.

Most intraspecific morphological and morphometrical differences presumably can be attributed to intraspecific variation (e.g., Mennecart and Costeur 2016; Schellhorn 2018) and the ecology of a species may be reflected in the degree of intraspecific variation of the bony labyrinth (e.g., Billet et al. 2012, Perier et al. 2016; Gonzales et al. 2019). In which way *P. pardus* differs from *P. leo* and *P. tigris* in these regards, should be investigated in the future. On an additional note, the available metadata of our sample do not suggest, that in mixing subspecies a pattern was obscured. However, this should be confirmed with much bigger samples.

In conclusion, the osseous secondary crus commune grundplan pattern of Felidae and their subfamilies needs to be discussed based on larger samples, especially to elucidate possible convergent character states.

We could not detect a secondary bony lamina of the cochlea in all our specimens which may be due to several reasons: intraspecific variation, scanning resolution and/or quality or simply possible lack of the character (e.g., *P. uncia*). This problem could be solved with an increased sample for each species of Pantherinae. In specimens for which we could trace the secondary bony lamina, its relative length is comparable to *Felis catus* whose lamina extends  $\frac{1}{2}$  a turn (Ekdale 2010, table 2). However, the drawing of the inner ear of *P. leo* provided by Hyrtl (1845, tab. IV fig. 12) suggests a secondary bony lamina, which reaches over  $\frac{3}{4}$  of a turn. In general, a long secondary bony lamina is associated with the ability to hear higher frequencies. The longer the secondary bony lamina is, the stiffer the basilar membrane, which is spanned between the secondary and the primary bony laminae (Ekdale 2010). Pantherinae live to some extent in vastly different habitats and hence different evolutionary constraints could lead to different hearing requirements (Sunquist and Sunquist 2002; Wilson and Mittermaier 2009; Ekdale 2010, 2013, 2016). A larger scale study investigating this aspect should be conducted in the future. For the discussion on the number of cochlear turns and aspect ratio of the cochlea see section Wild vs. captive specimens.

## Ontogenetic transformations

It is generally assumed that the bony labyrinth of neonate placental mammals already shows the maturity of adult stages in terms of size and shape and thus, it is justified to incorporate juvenile specimens in morphological and morphometric studies (e.g., Hoyte 1961; Pujol and Marty 1970; Tremble 1978; Richard et al. 2010; Mennecart and Costeur 2016; Costeur et al. 2019; Berlioz et al. 2021). However, some parts of the bony labyrinth still show postnatal growth until the petrosal bone is fully mature and recent studies on the bony labyrinth of *Orycteropus afer* and *Homo sapiens* reveal some postnatal changes of morphology (Richard et al. 2010; Berlioz et al. 2021; Bonczarowska et al. 2021). This is also supported by our results.

As observed in *P. leo* and *P. tigris* the absolute size of the bony labyrinth between neonate and adult stages is

very similar and the elongation of the canaliculus cochleae is obviously correlated with the expanding petrosal bone (see Fig. 5). In concert with this postnatal growth pattern a negative allometry of the bony labyrinth with the surrounding petrosal bone as well as the skull basal length can be observed during postnatal ontogeny as revealed by the decreasing IEH. Negative allometry of the mammalian inner ear with the body mass is well known when species of different size are compared: the larger the species the proportionally smaller the bony labyrinth (e.g., Spoor et al. 2007; Costeur et al. 2019). However, data on the relationship between bony labyrinth and the surrounding petrosal bone are scarce due to limited access to the respective structures. Based on modern imaging techniques the negative allometry of the bony labyrinth with the petrosal bone has been tested in fossil and extant mammals (e.g. Litopterna, Xenarthra, terrestrial Artiodactyla) (Billet et al. 2015; Mennecart and Costeur 2016). Thus, our observations on *P. leo* and *P. tigris* significantly contribute to a deeper understanding of the postnatal ontogenetic transformation of the inner ear. Even though, skull basal length of the infant *P. pardus* could not be determined, we confidently conclude that these allometric patterns are also present in *P. pardus* as well as in the other Pantherinae. This should be tested with a more comprehensive sample in terms of age stages as well as number of specimens.

In addition, the shape of the cochlea of *P. leo* also shows some postnatal changes in that higher aspect ratios are mostly found in the neonate and juvenile *P. leo* specimens (IDAS 1.1–1.3). The same trend has been observed in *Orycteropus afer*, in which the cochlea of young individuals is more conical than that of adults (Berlioz et al. 2021). The authors conclude that the cochlear shape is influenced by the surrounding bone and thus, in early postnatal stages the immature bony tissue allows more space for the cochlear apex. This could be also the case in *P. leo* although this needs to be examined on a greater sample size in order to rule out some intraspecific variation. However, delayed postnatal ossification in the cochlear apical area of the petrosal bone but without affecting the shape of the cochlea has also been described in some other placentals, e.g., *Felis catus* (Hoyte 1961; Pujol and Marty 1970; Richard et al. 2010).

The fossa subarcuata that houses the petrosal lobule of the cerebellar parafloculus is a plesiomorphic mammalian character (e.g., Hoyte 1961; Sánchez-Villagra 2002; Jeffery and Spoor 2006; Jeffery et al. 2008; Ruf et al. 2009, 2013; Ekdale 2010; Ekdale and Rowe 2011; Rodrigues et al. 2013; Billet et al. 2015). Its depth and size vary among species and still can change during postnatal ontogeny. For instance, in *Oryctolagus cuniculus* the fossa subarcuata increases rapidly in size by internal resorption of the bone and external appositional growth (Hoyte 1961) whereas it can become reduced or completely closed as observed, e.g., in some Primates, Proboscidea, Perissodactyla, and Artiodactyla (Gannon et al. 1988; Jeffery et al. 2008; Schmitt and Gheerbrandt 2016; Ali et al. 2021). Carnivora show a puzzling pattern with convergent closure of the fossa subarcuata in several clades. A distinct

fossa has been observed in Canidae, Ursidae, Ailuridae, Phocidae, Herpestidae, Viverridae, Hyaenidae (Gregory 1936; Gannon et al. 1988; Salles 1992; Ali et al. 2021). Closure of the fossa subarcuata leading to a shallow depression occurs in Otariidae, Odobenidae, *Ailuropoda melanoleuca*, *Procyon* sp., and Mustelidae; all species represented by infant and juvenile stages reveal the successive closure of the fossa by bony material (Gregory 1936; Wyss 1987; Gannon et al. 1988; Salles 1992). In Felidae the grundplan character is a distinct and deep fossa subarcuata as it is present in many species (Gannon et al. 1988; Salles 1992). Salles (1992) defines two different character states related to closure of the fossa: 1) highly reduced fossa, (2) residual depression whose systematic value is discussed. Character state (1) occurs in several feline species, e.g., *Leopardus tigrina*, *Prionailurus planiceps*, *Profelis temmincki*, *Pardofelis marmorata*, and character state (2) is present in, e.g., *Leopardus pardalis*, *Lynx rufus*, *Caracal caracal*, *Acinonyx jubatus* and all Pantherinae species (Salles 1992). However, *N. nebulosa* was not split into two species at that point in time (Buckley-Beason et al. 2006; Kitchener et al. 2006). It is obvious that the derived patterns defined by (Salles 1992) may not strictly reflect higher phylogenetic clades but species level as both characters can occur within one genus (see *Leopardus*).

Our observations on the postnatal increasing closure of the fossa subarcuata in *P. leo*, *P. tigris*, *P. pardus* support previous descriptions of this process in Carnivora although unfortunately no details on the age of the respective pantherine species in Salles (1992) is given; thus, our data may include the first observations for at least certain species of Pantherinae. Although our adult specimens all lost the fossa subarcuata they contradict the findings of Salles (1992) to some extent in that not all species show character stage (2) as proposed for Pantherinae. In *P. leo*, *P. tigris*, *P. uncia*, and most of the *P. pardus* specimens, the fossa subarcuata is completely reduced. However, one specimen of *P. pardus* (SMF 16529), *P. onca* and both *Neofelis* still have distinct but varying concavities in that area which resemble Salles' (1992) character state (1). If our observed differences reflect some intra-pantherine variation or heterochronic effects further studies of the ontogenetic change of the pantherine petrosal bone based on ontogenetic series are needed. In addition, these future studies may elucidate possible correlations of the fossa subarcuata and the ASC, i.e., if the fossa depth is influenced by the size (curvature) of the ASC (Billet et al. 2015) or vice versa (Jeffery and Spoor 2006; Jeffery et al. 2008). However, as the ASC limits the entrance into the fossa subarcuata, the depth of the latter may be caused by other constraints.

## Wild vs. captive specimens

Over several generations, captive specimens can show differences in their morphology, because of different constraints compared to the natural environment and thus, relaxation of evolutionary constraints can also affect the

vestibular organ including the bony labyrinth (O'Regan and Kitchener 2005; Billet et al. 2012).

Our study revealed that in *P. leo* and *P. tigris* the higher numbers of cochlear turns are found in the captive specimens, with the exception of SMF 4643 (*P. leo*). Interestingly, *P. pardus* features the opposite pattern, in which the captive specimens have fewer cochlear turns than the ones of wild origin.

Hyrtil (1845) reports 3 “full” turns of the cochlea for *P. leo* and *P. tigris*. Other studies report 2.75 turns of the cochlea for a captive *P. tigris* and a captive *P. onca* (Burda et al. 1984; Úlehlová et al. 1984).

Felids studied by Ekdale (2013), Etmayr (2014), Schellhorn (2018) and Grohé et al. (2018, fig. 2) all range between 3 and 3.25 cochlear turns. However, this does not hold true for all Carnivora. *Eumetopias jubatus* (Ekdale 2013, fig. 36D) shows around 2.25 turns, while Hyrtil (1845) reported 2 “full” turns for *Melursus ursinus*, *Phoca vitulina* and *Odobenus rosmarus*. In Mustelidae a wider range in cochlear turns is also present. Based on fig. 2 in Grohé et al. (2016) it ranges from around 2.75 to 4.25 between species. Traditionally, it is expected that the degree of coiling does not vary much in mammals (Ekdale and Rowe 2011; Ekdale 2016). However, there are exceptions observed in captive specimens: Ekdale (2010) reported variations in the number of cochlear turns of about 0.25 for captive *Monodelphis domestica*. In addition, Schellhorn (2018) stated that cochlear coiling in the domestic cat (*Felis catus*) shows the range of 3.00 to 3.25 turns. Furthermore, the inner ears of *Orycteropus afer* show a variation of 0.25 turns of the cochlea, although it is not apparent, which specimens are of wild and which are of captive origin (Berlioz et al. 2021, fig. 1).

In our sample the number of turns of the cochlea does not seem to correlate with the length of the cochlea in *P. leo*, *P. pardus* and *P. tigris*. However, the aspect ratio of the cochlea elucidates a certain pattern in *P. leo*: specimens with an aspect ratio of <0.6 have up to 3 cochlear turns, while specimens with >0.6 have more than 3 cochlear turns, albeit SMF 22104 (*P. leo*), which features 2.75 cochlear turns, has a higher aspect ratio as the *P. leo* specimens with 3 turns. Thus, captive *P. leo* specimens all have an aspect ratio >0.6, but it should be emphasized that our sample lacks adult lions from captive origin. In addition the presumably wild adult *P. leo* (SMF 4643) features 3.25 turns of the cochlea. The intraspecific differences in aspect ratio could be related to the tightness of coiling. Mennecart and Costeur (2016) explain the difference in the number of cochlear turns in *Tragulus kanchil* and *T. napu* by the tightness of the coiling, because the lengths of the cochlear canals are in the same range. Concerning number of cochlear turns captive specimens of *P. leo* and *P. tigris* show higher values than those from the wild. However, these specimens all represent neonate to infant stages. Thus, an ontogenetic patterning cannot be ruled out. Based on fig. 3 of Berlioz et al. (2021), post-natal subadult *Orycteropus afer* have up to 0.25 more cochlear turns than the adult specimens under study and, as discussed above, the aspect ratio can also change during ontogeny. This could also explain, why we see the op-

posite trend in *P. pardus*, in which case two of the adult specimens are from captive origin but show less cochlear turns than the infant wild specimen under study.

Based on this approach, in future studies the tightness of the cochlear coiling along the ontogenetic sequence from wild and captive Pantherinae should be systematically investigated with a much larger sample. Additional morphometric measurements, e.g., the laminar gap and cochlear volume, should be carried out in the future as well. This could help to elucidate the developmental or evolutionary drivers for different cochlear turn numbers and cochlear shape between wild and captive specimens.

## Conclusion

The inner ear is a sensory organ, which is exposed to high evolutionary constraints (Billet et al. 2012). This is reflected in the morphology of the bony labyrinths in our Pantherinae sample. While closely related, there are subtle, but clearly noticeable morphological differences within the Pantherinae species, which may be caused by different habitats and behavior (Wilson and Mittermeier 2009; Ekdale 2013, 2016). However, elucidating the morphofunctional and/or phylogenetic relationships of these features, still needs to be done with much larger sample sizes in the future.

We were able to show a negative allometry of the bony labyrinth with the skull basal length between larger and smaller Pantherinae species. In case of the genus *Neofelis*, the large size difference likely also has a functional component (Spoor et al. 2007). A negative allometry of the bony labyrinth is also present during ontogeny, with the petrosal bone and entire skull increasing in size, while the size of the bony labyrinth nearly stays the same. We traced this in different ontogenetic stages in *P. leo*, but are confident, that it is also true for the other Pantherinae species. A good indicator for a rough age estimation is the relative size of the canaliculus cochleae, which increases in length during ontogeny.

The size of our sample was not sufficient for a statistical analysis and proper discussion of intraspecific variation, albeit we presented certain patterns, which should be investigated further in the future. The same holds true for the comparison of bony labyrinth morphology of wild and captive animals.

## Funding

This research has been supported by the Paul-Ungerer-Stiftung and Seiko Deutschland Branch of SEIKO Watch Europe B.V.

## Acknowledgements

The authors thank Katrin Krohmann, Juliane Eberhardt (both SGN Frankfurt), Rachel A. Racicot (Vanderbilt University, Nashville, Ten-

nessee), Franziska Fritzsche, Antonia Späth, and Franziska Wagner (all formerly SGN Frankfurt) for technical support. Special thanks go to Patrick Bak (Yxlon International GmbH, Hamburg) for providing the  $\mu$ CT scan of one specimen. Special thanks go to Guillaume Billet and two anonymous reviewers who helped to improve the manuscript.

## References

- Anders U, von Koenigswald W, Ruf I, Smith, BH (2011) Generalized individual dental age stages for fossil and extant placental mammals. *Paläontologische Zeitschrift* 85(3): 321–339. <https://doi.org/10.1007/s12542-011-0098-9>
- Ali S, Esmat A, Erasha AM (2021) Contribution on the size and morphology of subarcuate fossa in some mammals and its implications to phylogeny. *SVU-International Journal of Veterinary Sciences* 4(2): 27–34. <https://doi.org/10.21608/svu.2021.60109.1103>
- Berlioz E, Cornette R, Lenoir N, Santin MD, Lehmann T (2021) Exploring the ontogenetic development of the inner ear in Aardvarks. *Journal of Anatomy* 238(5): 1128–1142. <https://doi.org/10.1111/joa.13361>
- Billet G, Muizon CD (2013) External and internal anatomy of a petrosal from the late Paleocene of Itaboraí, Brazil, referred to Notoungulata (Placentalia). *Journal of Vertebrate Paleontology* 33(2): 455–469. <https://doi.org/10.1080/02724634.2013.722153>
- Billet G, Hautier L, Asher RJ, Schwarz C, Crumpton N, Martin T, Ruf I (2012) High morphological variation of vestibular system accompanies slow and infrequent locomotion in three-toed sloths. *Proceedings of the Royal Society B: Biological Sciences* 279(1744): 3932–3939. <https://doi.org/10.1098/rspb.2012.1212>
- Billet G, Germain D, Ruf I, de Muizon C, Hautier L (2013) Inner ear morphology in *Megatherium* and insights on the evolution of vestibular system and locomotion in sloths. *Journal of Anatomy* 223: 557–567. <https://doi.org/10.1111/joa.12114>
- Billet G, De Muizon C, Schellhorn R, Ruf I, Ladevèze S, Bergqvist L (2015) Petrosal and inner ear anatomy and allometry amongst specimens referred to Litopterna (Placentalia). *Zoological Journal of the Linnean Society* 173(4): 956–987. <https://doi.org/10.1111/zoj.12219>
- Bonczarowska JH, Spanakis K, Kranioti EF (2021) Postnatal changes of the human bony labyrinth morphology. *Homo: Internationale Zeitschrift für die Vergleichende Forschung am Menschen* 72(3): 229–238. <https://doi.org/10.1127/homo/2021/1365>
- Buckley-Beason VA, Johnson WE, Nash WG, Stanyon R, Menninger JC, Driscoll CA, Howard J, Bush M, Page JE, Roelke ME, Stone G, Martelli PP, Wen C, Ling L, Duraisingam RK, Lam PV, O'Brien SJ (2006) Molecular evidence for species-level distinctions in clouded leopards. *Current Biology* 16(23): 2371–2376. <https://doi.org/10.1016/j.cub.2006.08.066>
- Burda H, Úřelová L, Branis M (1984) Morphology of the middle and inner ear in *Panthera* species—*P. tigris* and *P. onca* (Felidae, Carnivora, Mammalia). *Vestník Československé Zoologické Společnosti* 48: 9–14.
- Cerio DG, Witmer LM (2019) Intraspecific variation and symmetry of the inner-ear labyrinth in a population of wild turkeys: Implications for paleontological reconstructions. *PeerJ* 7: 1–26. <https://doi.org/10.7717/peerj.7355>
- Costeur L, Mennecart B, Müller B, Schulz G (2017) Prenatal growth stages show the development of the ruminant bony labyrinth and petrosal bone. *Journal of Anatomy* 230(2): 347–353. <https://doi.org/10.1111/joa.12549>
- Costeur L, Mennecart B, Müller B, Schulz G (2019) Observations on the scaling relationship between bony labyrinth, skull size and body mass in ruminants. In: Müller B, Wang E (Eds) *Developments in X-Ray Tomography XII* (Vol. 11113). SPIE Optical Engineering + Applications, San Diego (California, United States), August 2019. International Society for Optics and Photonics, San Diego: 1111313. <https://doi.org/10.1117/12.2530702>
- Crégut-Bonnouere E, Boulbes N, Desclaux E, Marciszak A (2018) New insights into the LGM and LG in Southern France (Vaucluse): the mustelids, micromammals and horses from Coulet des Roches. *Quaternary* 1(3): 19. <https://doi.org/10.3390/quat1030019>
- Davis BW, Li G, Murphy WJ (2010) Supermatrix and species tree methods resolve phylogenetic relationships within the big cats, *Panthera* (Carnivora: Felidae). *Molecular Phylogenetics and Evolution* 56(1): 64–76. <https://doi.org/10.1016/j.ympev.2010.01.036>
- Ekdale EG (2010) Ontogenetic variation in the bony labyrinth of *Mondelphis domestica* (Mammalia: Marsupialia) following ossification of the inner ear cavities. *The Anatomical Record* 293(11): 1896–1912. <https://doi.org/10.1002/ar.21234>
- Ekdale EG (2013) Comparative anatomy of the bony labyrinth (inner ear) of placental mammals. *PLoS One* 8(6): e66624. <https://doi.org/10.1371/journal.pone.0137149>
- Ekdale EG (2016) Form and function of the mammalian inner ear. *Journal of Anatomy* 228: 324–337. <https://doi.org/10.1111/joa.12308>
- Ekdale EG, Rowe T (2011) Morphology and variation within the bony labyrinth of zhelestids (Mammalia, Eutheria) and other therian mammals. *Journal of Vertebrate Paleontology* 31(3): 658–675. <https://doi.org/10.1080/02724634.2011.557284>
- Etmayr L (2014) Das Mittel- und Innenohr von ausgewählten Feliden (*Felis chaus*, *Puma concolor*, *Caracal caracal*, *Prionailurus viverrinus*) – 3D-Rekonstruktionen. Diploma thesis, Universität Wien, Vienna, Austria. <https://doi.org/10.25365/thesis.33325>
- Gannon PJ, Eden AR, Laitman JT (1988) The subarcuate fossa and cerebellum of extant primates: comparative study of a skull-brain interface. *American Journal of Physical Anthropology* 77: 143–164. <https://doi.org/10.1002/ajpa.1330770202>
- Gonzales LA, Malinzak MD, Kay RF (2019) Intraspecific variation in semicircular canal morphology—A missing element in adaptive scenarios? *American Journal of Physical Anthropology* 168(1): 10–24. <https://doi.org/10.1002/ajpa.23692>
- Gregory, WK (1936). On the phylogenetic relationships of the giant panda (Ailuropoda) to other arctoid Carnivora. *American Museum Novitates* 878: 1–29. <https://core.ac.uk/download/pdf/18226579.pdf>
- Grohé C, Tseng ZJ, Lebrun R, Boistel R, Flynn JJ (2016) Bony labyrinth shape variation in extant Carnivora: a case study of Musteloidea. *Journal of Anatomy* 228(3): 366–383. <https://doi.org/10.1111/joa.12421>
- Grohé C, Lee B, Flynn JJ (2018) Recent inner ear specialization for high-speed hunting in cheetahs. *Scientific Reports* 8(1): 1–8. <https://doi.org/10.1038/s41598-018-20198-3>
- Hammer Ø (2020) PAST 4.03, available online: <https://www.freeware-base.de/freeware-zeige-details-31687-Past.html> (accessed on June 19<sup>th</sup>, 2022).
- Hammer Ø, Harper DAT, Ryan, PD (2001) PAST: Paleontological Statistics software package for education and data analysis. *Palaeontologia Electronica* 4(1): 1–9. [http://palaeo-electronica.org/2001\\_1/past/issue1\\_01.htm](http://palaeo-electronica.org/2001_1/past/issue1_01.htm)
- Hemmer H (1968) Untersuchungen zur Stammesgeschichte der Pantherkatzen (Pantherinae) Teil II Studien zur Ethologie des Nebelparders „*Neofelis nebulosa*“ (Griffith 1821) und des Irbis „*Uncia*

- uncia*“ (Schreber 1775). Veröffentlichungen der Zoologischen Staatssammlung München 12: 155–247. [https://www.zobodat.at/pdf/VeroeffZSM\\_012\\_0155-0247.pdf](https://www.zobodat.at/pdf/VeroeffZSM_012_0155-0247.pdf)
- Hoyle (1961) The postnatal growth of the ear capsule in the rabbit. *American Journal of Anatomy* 108(1): 1–16. <https://doi.org/10.1002/aja.1001080102>
- Hyrtil J (1845) Vergleichend-anatomische Untersuchungen über das innere Gehörorgan des Menschen und der Säugethiere: Mit neun Kupfertafeln, Verlag von Friedrich Ehrlich, Prag, 139 pp.
- Jeffery N, Spoor F (2004) Prenatal growth and development of the modern human labyrinth. *Journal of Anatomy* 204(2): 71–92. <https://doi.org/10.1111/j.1469-7580.2004.00250.x>
- Jeffery N, Spoor F (2006) The primate subarcuate fossa and its relationship to the semicircular canals part I: prenatal growth. *Journal of human evolution* 51(5): 537–549. <https://doi.org/10.1016/j.jhevol.2006.07.003>
- Jeffery N, Ryan TM, Spoor F (2008) The primate subarcuate fossa and its relationship to the semicircular canals part II: adult interspecific variation. *Journal of human evolution* 55(2): 326–339. <https://doi.org/10.1016/j.jhevol.2008.02.010>
- Jiangzuo Q, Liu J (2020) First record of the Eurasian jaguar in southern Asia and a review of dental differences between pantherine cats. *Journal of Quaternary Science* 35(6): 817–830. <https://doi.org/10.1002/jqs.3222>
- Johnsson LG, Hawkins JE (1967) A direct approach to cochlear anatomy and pathology in man. *Archives of Otolaryngology* 85(6): 599–613. <https://doi.org/10.1001/archotol.1967.00760040601005>
- Kitchener AC, Beaumont MA, Richardson D (2006) Geographical variation in the clouded leopard, *Neofelis nebulosa*, reveals two species. *Current Biology* 16(23): 2377–2383. <https://doi.org/10.1016/j.cub.2006.10.066>
- Kitchener AC, Breitenmoser-Würsten C, Eizirik E, Gentry A, Werdelin L, Wilting A, Yamaguchi N, Abramov AV, Christiansen P, Driscoll C, Duckworth JW, Johnson W, Luo S-J, Meijaard E, O’Donoghue P, Sanderson J, Seymour K, Bruford M, Groves C, Hoffmann M, Nowell K, Timmons Z, Tobe S (2017) A revised taxonomy of the Felidae. The final report of the Cat Classification Task Force of the IUCN/ SSC Cat Specialist Group, *Cat News Special* 11: 80 pp. <https://repository.si.edu/handle/10088/32616>
- Luo Z-X, Ruf I, Martin T (2012) The petrosal and inner ear of the Late Jurassic cladotherian mammal *Dryolestes leiriensis* and implications for ear evolution in therian mammals. *Zoological Journal of the Linnean Society* 166(2): 433–463. <https://doi.org/10.1111/j.1096-3642.2012.00852.x>
- Maier W, Ruf I (2014) Morphology of the nasal capsule of Primates— with special reference to *Daubentonia* and *Homo*. *The Anatomical Record* 297(11): 1985–2006. <https://doi.org/10.1002/ar.23023>
- Mennecart B, Costeur L (2016) Shape variation and ontogeny of the ruminant bony labyrinth, an example in Tragulidae. *Journal of Anatomy* 229(3): 422–435. <https://doi.org/10.1111/joa.12487>
- Mennecart B, Rössner GE, Métais G, DeMiguel D, Schulz G, Müller B, Costeur L (2016) The petrosal bone and bony labyrinth of early to middle Miocene European deer (Mammalia, Cervidae) reveal their phylogeny. *Journal of Morphology* 277(10): 1329–1338. <https://doi.org/10.1002/jmor.20579>
- Morsli H, Choo D, Ryan A, Johnson R, Wu DK (1998) Development of the mouse inner ear and origin of its sensory organs. *Journal of Neuroscience* 18(9): 3327–3335. <https://doi.org/10.1523/JNEUROSCI.18-09-03327.1998>
- Nowak RM (1991) Walker’s Mammals of the World, Volume II, Fifth Edition. The Johns Hopkins University Press, Baltimore and London, 987 pp.
- O’Regan HJ, Kitchener AC (2005) The effects of captivity on the morphology of captive, domesticated and feral mammals. *Mammal Review* 35(3–4): 215–230. <https://doi.org/10.1111/j.1365-2907.20-05.00070.x>
- Perier A, Lebrun R, Marivaux L (2016) Different level of intraspecific variation of the bony labyrinth morphology in slow- versus fast-moving primates. *Journal of Mammalian Evolution* 23: 353–368. <https://doi.org/10.1007/s10914-016-9323-3>
- Pfaff C, Martin T, Ruf I (2015) Bony labyrinth morphometry indicates locomotor adaptations in the squirrel-related clade (Rodentia, Mammalia). *Proceedings of the Royal Society B: Biological Sciences* 282(1809): 20150744. <https://doi.org/10.1098/rspb.2015.0744>
- Pfaff C, Czerny S, Nagel D, Kriwet J (2017) Functional morphological adaptations of the bony labyrinth in marsupials (Mammalia, Theria). *Journal of Morphology* 278(6): 742–749. <https://doi.org/10.1002/jmor.20669>
- Pujol R, Marty R (1970) Postnatal maturation in the cochlea of the cat. *Journal of Comparative Neurology* 139(1): 115–125. <https://doi.org/10.1002/cne.901390108>
- Richard C, Laroche N, Malaval L, Dumollard JM, Martin C, Peoch M, Vico L, Prades JM (2010) New insight into the bony labyrinth: a microcomputed tomography study. *Auris Nasus Larynx* 37(2): 155–161. <https://doi.org/10.1016/j.anl.2009.04.014>
- Rodrigues PG, Ruf I, Schultz CL (2013) Digital reconstruction of the otic region and inner ear of the non-mammalian cynodont *Brasilitherium riograndensis* (Late Triassic, Brazil) and its relevance to the evolution of the mammalian ear. *Journal of Mammalian Evolution* 20(4): 291–307. <https://doi.org/10.1007/s10914-012-9221-2>
- Ruf I, Luo Z-X, Martin T (2013) Reinvestigation of the basicranium of *Haldanodon expectatus* (Mammaliaformes, Docodonta). *Journal of Vertebrate Paleontology* 33(2): 382–400. <https://doi.org/10.1080/02724634.2013.722575>
- Ruf I, Luo Z-X, Wible JR, Martin T (2009) Petrosal anatomy and inner ear structures of the Late Jurassic *Henkelotherium* (Mammalia, Cladotheria, Dryolestidae): insight into the early evolution of the ear region in cladotherian mammals. *Journal of Anatomy* 214: 679–693. <https://doi.org/10.1111/j.1469-7580.2009.01059.x>
- Ruf I, Volpato V, Rose KD, Billet G, de Muizon C, Lehmann T (2016) Digital reconstruction of the inner ear of *Leptictidium auderiense* (Leptictida, Mammalia) and North American leptictids reveals new insight into leptictidan locomotor agility. *Paläontologische Zeitschrift* 90: 153–171. <https://doi.org/10.1007/s12542-015-0276-2>
- Salles LO (1992) Felid phylogenetics: extant taxa and skull morphology (Felidae, Aeluroidea). *American Museum Novitates* 3047: 1–67. <https://digitallibrary.amnh.org/bitstream/handle/2246/5011/v2/dspace/ingest/pdfSource/nov/N3047.pdf?sequence=1&isAllowed=y>
- Sánchez-Villagra MR (2002) The cerebellar paraflocculus and the subarcuate fossa in *Monodelphis domestica* and other marsupial mammals—ontogeny and phylogeny of a brain-skull interaction. *Acta Theriologica* 47(1): 1–14. <https://doi.org/10.1007/BF03193561>
- Sánchez-Villagra MR, Schmelzle T (2007) Anatomy and development of the bony inner ear in the woolly opossum, *Caluromys philander* (Didelphimorphia, Marsupialia). *Mastozoología Neotropical* 14: 53–60. <http://www.scielo.org.ar/pdf/mznt/v14n1/v14a06.pdf>
- Segura V, Cassini GH, Prevosti FJ (2017) Three-dimensional cranial ontogeny in pantherines (*Panthera leo*, *P. onca*, *P. pardus*, *P. tigris*)

- gris*; Carnivora: Felidae). *Biological Journal of the Linnean Society* 120(1): 210–227. <https://doi.org/10.1111/bij.12888>
- Schmitt A, Gheerbrant E (2016) The ear region of earliest known elephant relatives: new light on the ancestral morphotype of proboscideans and afrotherians. *Journal of Anatomy* 228(1): 137–152. <https://doi.org/10.1111/joa.12396>
- Schellhorn R (2018) Intraspecific variation in the domestic cat bony labyrinth revealed by different measurement techniques. *Journal of Morphology* 279: 409–417. <https://doi.org/10.1002/jmor.20781>
- Schwab JA, Kriwet J, Weber GW, Pfaff C (2019) Carnivoran hunting style and phylogeny reflected in bony labyrinth morphometry. *Scientific Reports* 9: 1–9. <https://doi.org/10.1038/s41598-018-37106-4>
- Schmelzle T, Sánchez-Villagra MR, Maier W (2007) Vestibular labyrinth diversity in diprotodontian marsupial mammals. *Mammal Study* 32: 83–97. [https://doi.org/10.3106/1348-6160\(2007\)32\[83:VLDIDM\]2.0.CO;2](https://doi.org/10.3106/1348-6160(2007)32[83:VLDIDM]2.0.CO;2)
- Schwarz C (2012) Phylogenetische und funktionsmorphologische Untersuchungen der Ohrregion bei Sciuromorpha (Rodentia, Mammalia). PhD Thesis, Rheinische Friedrich-Wilhelms-Universität Bonn, Bonn, Germany. <https://bonndoc.ulb.uni-bonn.de/xmloi/handle/20.500.11811/5366>
- Smuts GL, Anderson JL, Austin JC (1978) Age determination of the African lion (*Panthera leo*). *Journal of Zoology* 185(1): 115–146. <https://doi.org/10.1111/j.1469-7998.1978.tb03317.x>
- Spoor F, Garland Jr T, Krovitz G, Ryan TM, Silcox MT, Walker A (2007) The primate semicircular canal system and locomotion. *Proceedings of the National Academy of Sciences of the United States of America* 104: 10808–10812. <https://doi.org/10.1073/pnas.0704250104>
- Sunquist M, Sunquist F (2002) *Wild Cats of the World*. University of Chicago Press, Chicago and London, 542 pp.
- Tremble GE (1978) Size of bony labyrinth of human infant and adult compared to that in certain animals. *Annals of Otology, Rhinology & Laryngology* 87(3): 351–355. <https://doi.org/10.1177/0003489-47808700310>
- Úlehlová L, Burda H, Voldřich L (1984) Involution of the auditory neuro-epithelium in a tiger (*Panthera tigris*) and a jaguar (*Panthera onca*). *Journal of Comparative Pathology* 94(1): 153–157. [https://doi.org/10.1016/0021-9975\(84\)90017-3](https://doi.org/10.1016/0021-9975(84)90017-3)
- West CD (1985) The relationship of the spiral turns of the cochlea and the length of the basilar membrane to the range of audible frequencies in ground dwelling mammals. *Journal of the Acoustic Society of America* 77: 1091–1101. <https://doi.org/10.1121/1.392227>
- Wible JR, Shelley SL (2020) Anatomy of the petrosal and middle ear of the brown rat, *Rattus norvegicus* (Berkenhout, 1769) (Rodentia, Muridae). *Annals of Carnegie Museum* 86(1): 1–35. <https://doi.org/10.2992/007.086.0101>
- Wible JR, Rougier GW, Novacek MJ, Asher RJ (2009) The eutherian mammal *Maelestes gobiensis* from the Late Cretaceous of Mongolia and the phylogeny of Cretaceous Eutheria. *Bulletin of the American Museum of Natural History* 209(327): 1–123. <https://doi.org/10.1206/623.1>
- Wilson DE, Mittermeier RA (2009) *Handbook of the Mammals of the World – Volume 1 Carnivores*. Lynx Edicions in association with Conservation International and IUCN, Barcelona, 728 pp.
- Wyss AR (1987). The walrus auditory region and the monophyly of pinnipeds. *American Museum Novitates* 2871: 1–31. <https://digitalibrary.amnh.org/bitstream/handle/2246/5195/v2/dspace/ingest/pdfSource/nov/N2871.pdf?sequence=1&isAllowed=y>

## Supplementary material 1

### Tables S1, S2

**Authors:** Wirkner M, Heyder K, Ruf I (2022)

**Data type:** .xlsx

**Explanation note:** **Table S1.**  $\mu$ CT scan parameters of studied Pantherinae. For some specimens the resolution has been virtually increased (res 2). — **Table S2.** Raw measurements of the studied Pantherinae specimens. Abbreviations: ASC, anterior semicircular canal; BL, skull basal length; cco, canaliculus cochleae; co, cochlea; H, height; IEH, inner ear height; iH, inner height; iW, inner width; L, length; l, left; LSC, lateral semicircular canal; oH, outer height; oW, outer width; PSC, posterior semicircular canal r, right; W, width.

**Copyright notice:** This dataset is made available under the Open Database License (<http://opendatacommons.org/licenses/odbl/1.0>). The Open Database License (ODbL) is a license agreement intended to allow users to freely share, modify, and use this Dataset while maintaining this same freedom for others, provided that the original source and author(s) are credited.

**Link:** <https://doi.org/10.3897/vz.72.e82874.suppl1>

## Supplementary material 2

### Figures S1–S5

**Authors:** Wirkner M, Heyder K, Ruf I (2022)

**Data type:** .pdf

**Explanation note:** **S1** Virtual endocasts of the right bony labyrinth of *Panthera leo*. **A–D** SMF 22101; **E–H** SMF 22104; **I–L** SMF 1366, left side mirrored. All depicted individuals are adult. Abbreviations: aa, anterior ampulla; acf, aperture of the cochlear fossula; ASC, anterior semicircular canal; av, aquaeductus vestibuli; bp, bony protuberance; cc, crus commune; cco, canaliculus cochleae; co, cochlea; fv, fenestra vestibuli; la, lateral ampulla; LSC, lateral semicircular canal; pa, posterior ampulla; PSC, posterior semicircular canal; sbl, secondary bony lamina; scc, secondary crus commune. Scale bar: 5 mm. — **S2** Ontogenetic transformations of the radius of curvature in the bony labyrinth of *Panthera leo*, *P. pardus* and *P. tigris*. The values of species are averaged. **A** *P. leo* (n=4), **B** *P. tigris* (n=3), **C** *P. pardus* (n=2). Abbreviations: ASC, anterior semicircular canal; co-L, cochlear length; IEH, inner ear height; LSC, lateral semicircular canal; PSC, posterior semicircular canal; R, radius of curvature. — **S3** Virtual endocasts of the right bony labyrinth of selected *Panthera* species. **A–D** *Panthera pardus* SMF 94342; **E–H** *P. pardus* SMF 95992, left side mirrored; **I–L** *P. tigris* SMF 7020. All depicted individuals are adult. Abbreviations: aa, anterior ampulla; acf, aperture of the cochlear fossula; ASC, anterior semicircular canal; av, aquaeductus vestibuli; bp, bony protuberance; cc, crus commune; cco, canaliculus cochleae; co, cochlea; fv, fenestra vestibuli; la, lateral ampulla; LSC, lateral semicircular canal; pa, posterior ampulla; PSC, posterior semicircular canal. Scale bars: 5 mm. — **S4** Dorsal view of right bony labyrinth endocasts of *Panthera* species illustrating differences in the secondary crus commune. **A** *Panthera pardus* (SMF 95992, left side mirrored), **B** *P. onca* (SMF 3067), **C** *P. leo* (SMF 4643), **D** *P. uncia* (SMF 5419, left side mirrored), **E** *P. tigris* (SMF 15737). Abbreviations: aa, anterior ampulla; acf, aperture of the cochlear fossula; ASC, anterior semicircular canal; bv, canal for blood vessels; cc, crus commune; cco, canaliculus cochleae; co, cochlea; de, dorsal extension of the aperture of the cochlear fossula; la, lateral ampulla; LSC, lateral semicircular canal; pa, posterior ampulla; PSC, posterior semicircular canal; scc, secondary crus commune. Scale bar: 5 mm. — **S5** Size comparison of selected structures standardized by inner ear height in adult stages of all studied Pantherinae species. The linear equation, the coefficient of determination ( $R^2$ ) and the p-value are given in the respective graph. **A** cochlear length, **B** anterior semicircular canal radius of curvature, **C** lateral semicircular canal radius of curvature, **D** posterior semicircular canal radius of curvature. Abbreviations: ASC, anterior semicircular canal; co-L, cochlear length; IEH, inner ear height; LSC, lateral semicircular canal; PSC, posterior semicircular canal; R, radius of curvature.

**Copyright notice:** This dataset is made available under the Open Database License (<http://opendatacommons.org/licenses/odbl/1.0>). The Open Database License (ODbL) is a license agreement intended to allow users to freely share, modify, and use this Dataset while maintaining this same freedom for others, provided that the original source and author(s) are credited.

**Link:** <https://doi.org/10.3897/vz.72.e82874.suppl2>